Student thesis series INES nr 543

Analysis of coastal erosion between different flights of UAV

Zhengran Yin

2021
Department of
Physical Geography and Ecosystem Science
Lund University
Sölvegatan 12
S-223 62 Lund
Sweden

Zhengran Yin (2021).

Analysis of Coastal Erosion between Different flights of UAV

Analys av kusterosion mellan olika flygningar med UAV

Master degree thesis, 30 credits in *Geomatics*

Department of Physical Geography and Ecosystem Science, Lund University

Level: Master of Science (MSc)

Course duration: *January* 2021 until *June* 2021

Disclaimer

This document describes work undertaken as part of a program of study at the University of Lund. All views and opinions expressed herein remain the sole responsibility of the author and do not necessarily represent those of the institute.

Analysis of Coastal Erosion between Different flights of UAV

Zhengran Yin

Master thesis, 30 credits, in *Geomatics*

Per-Ola Olsson

Lund University

Exam committee:

Helena Elvén Eriksson, Lund University

Pengxiang Zhao, Lund University

Abstract

More than 600 million people are living in coastal areas in the world. According to the trend of population migration, the global coastal area population may increase to more than 1 billion by 2050. In a long term, a series of activities such as sea-level rise due to global warming and unpredictable natural disasters increase the extent of coastal erosion. As coastal erosion continues to intensify, it may cause erosion of soil resources and threaten the safety of coastal buildings and roads. This series of damages to human life and economic property caused by coastal erosion make it important to monitor coastal erosion. Traditional collection methods like peg-lines, total station, Terrestrial Laser Scanning (TLS), airborne LiDAR (Light Detection and Ranging), Global Navigation Satellite System (GNSS) surveys and aerial imagery can obtain high-resolution data. Although the accuracy of the monitoring can meet the requirements, the disadvantage is that the cost is high, and it is difficult to carry out long-term multiple coastal erosion monitoring. Compared to traditional monitoring methods, the use of UAV for images collection is low in cost, easy to operate and has fewer limitations. UAV has the characteristics of low-cost equipment and a high degree of automation, which makes it advantageous when monitoring coastal erosion. Therefore, in this study, a digital surface model (DSM), an elevation difference map, a DSM accuracy map and a slope map were created based on five UAV images at different times. According to the obtained elevation difference map and accuracy map, the degree of coastal erosion can be quantified, and the seasonal pattern and spatial pattern of coastal erosion can be obtained. However, due to the limitation of the error and other uncertain values in the DSM in this project, the elevation difference in the study area does not completely represent the elevation change, that is, the value of coastal erosion. Therefore, it is also necessary to remove or reduce the influence of uncertain values in the research.

Keywords: Coastal erosion, UAV, Digital Surface Model, Slope, Elevation differences.

Acknowledgement

First, I want to express gratitude to my supervisors Per-Ola Olsson for their outstanding encouragement, technical insights, and critical feedback throughout this project, and to Kristiansads Kummun for providing UAV images, GCP coordinates and weather condition. Moreover, I want to thank everyone at the department at Lund University for enabling me to succeed in my studies. And I want to thank my friends and family for providing me with continuous support.

This project used UAV images of a beach area in Åhus, including the following times: October 2017, April 2019, December 2019, March 2020, May 2020.

Table of Contents

List of Figures

List of Tables

List of Abbreviations

1.	DSM	Digital Surface Model
2.	TLS	Terrestrial Laser Scanning
3.	ATV	All-terrain vehicle
4.	UAV	Unmanned Aerial Vehicle
5.	LiDAR	Light detection and ranging
6.	GNSS	Global Navigation Satellite System
7.	SfM	Structure from Motion
8.	DEM	Digital Elevation Models

1.Introduction

More than 600 million people are living in coastal areas in the world. According to the trend of population migration, the global coastal area population may increase to more than 1 billion by 2050 (Neumann et al., 2015; Merkens et al., 2016). Over time, the coastline is affected by natural factors such as waves, tides, or storms, resulting in soil loss or rock loss (Yoo and Oh, 2016). In a long term, a series of activities such as sea-level rise due to global warming (Cooper and Lemckert, 2012) and unpredictable natural disasters increase the extent of coastal erosion. As coastal erosion continues to intensify, it may cause erosion of soil resources and threaten the safety of coastal buildings and roads. A study by Zhang et al. (2004) stated that long-term coastal erosion is affected by sea-level rise, and the gradual increase in coastal erosion will directly damage nearby fixed structures. Reid and Mathews. (1906) reported substantial annual losses of land due to coastal erosion, and features such as the contour and cross-section of the coast are changing. This series of damages to human life and economic property caused by coastal erosion make it important to monitor coastal erosion.

One common method to monitor coastal erosion is to perform change analyses with Digital Surface Models (DSMs) obtained at different times. Mostly DSMs represent the earth's surface and include all objects on it, which is to express the spatial distribution of actual terrain features in the form of numbers. In this field, the commonly used traditional monitoring techniques are Terrestrial Laser Scanning (TLS), GPS surveying, total station, and All-terrain vehicle (ATV) (Turner et al., 2016). However, these traditional surveillance technologies have a low spatial resolution or high cost. The products obtained through these technologies have another shortcoming, that is, the obtained data sets do not contain orthophotos, which can be used to study terrain from other aspects, for example, to monitor changes (Tak et al., 2020). It would be a major advantage with a method that provides both orthophotos and DSMs.

The rapid development of Unmanned Aerial Vehicle (UAV) technology makes UAV a

good solution for coastal erosion monitoring. UAV provides an efficient and cheap data collection method that can facilitate the production of high spatiotemporal resolution DSMs. Compared to other surveying equipment, UAV is inexpensive, so the biggest advantage of UAV in coastal erosion monitoring applications is the relatively low cost of hardware facilities, easy operation, the high automation level of data collection and high spatial resolution (Goncalves and Henriques, 2015). Long et al (2016) stated that UAV can be used to produce DSMs with similar accuracy as traditional light detection and ranging (LiDAR) which have been used for decades (Haala and Rothermel, 2012). Another advantage of using UAV is that both DSM and orthophotos can be created (Lee et al., 2019). These features make UAV a reliable tool for beach/sand erosion monitoring applications.

Aim and research questions

This project aims to process UAV image data from the municipality of Kristianstad to create Digital Surface Models (DSMs) and to assess the ability to quantitatively analyze the coastal erosion along the sandy beach. Both spatial and temporal changes will be studied in this project.

The specific research questions are:

1. What are the elevation changes of the study area in different time gaps?
2. Is there any seasonal pattern in changes?
3. Is there any spatial pattern in changes?

2. Background

2.1 Coastal Erosion

Under the continuous action of natural factors such as wind and waves, there are inflows and expenditures of marine sediment along the coastline. When the expenditure is greater than the inflow, the beach and coastline will move back or erode as a result, which is called coastal erosion (Yoo & Oh, 2016). The marine erosion damage to the coast is mainly divided into mechanical erosion and dissolution. Mechanical erosion is mainly due to the damaging effects of sea wave motions and tide on the coast (Leo,1993). Mechanical erosion mainly includes corrosion, abrasion, hydraulic action and attrition. The process of Corrosion is that the material (stone) on the beach is picked up by the wave and thrown to the bottom. Abrasion is usually called the sandpaper effect, which usually occurs when the waves enveloping the sand and other sediments erode the beach. Hydraulic action generally occurs in coastal areas with cliffs; Air is compressed into cracks when the wave hits the bottom of the cliff and when the wave retreats, the air in the crack causes the surface of the cliff to fall off. Attrition is because of the action of the wave, the small pebbles collide and break. Dissolution is because seawater contains more solvents such as CO_2, which will dissolve coastal and seabed rocks (Rosser et al., 2005).

In this project, the main research area is a sandy coast; hence, only the erosion process of sandy coasts is described in detail. Rijn (2011) stated that the erosion process of sandy coasts is different from other erosion processes because sandy coasts are composed of loose sand grains and the terrain is relatively flat. The main driving forces for the erosion of sandy coasts are waves and tides. In the erosion process, the energy generated by the waves, currents and water accumulated on the beach cannot reach a balanced state, so the beach will lose sediments, which will cause the beach to continue to retreat. In general, the imbalance of energy input, beach resistance and the imbalance of sediments that are easily moved by water is considered to be the cause of beach erosion. (Anthony, 2019) Longshore drifting (Figure2.1) is a relatively common

phenomenon. Longshore drifting is the phenomenon of the material moving along the coast when there is a certain angle between the direction of wave movement and the coast (Niven & Bardsley, 2012). Longshore current is affected by the speed of the waves, the angle of the waves, the length of the beach, and the shape of the beach. When waves hit the beach at a steep angle, the speed of the Longshore current is higher; when waves hit the beach at a gentle angle, the speed of the Longshore current is lower. In addition, the longer and straighter the beach, the stronger the Longshore current (National Ocean Service, 2017). Inflows and tidal currents drive sand toward the coast, while undercurrents bring some sand back into the sea (Rijn, 2011).

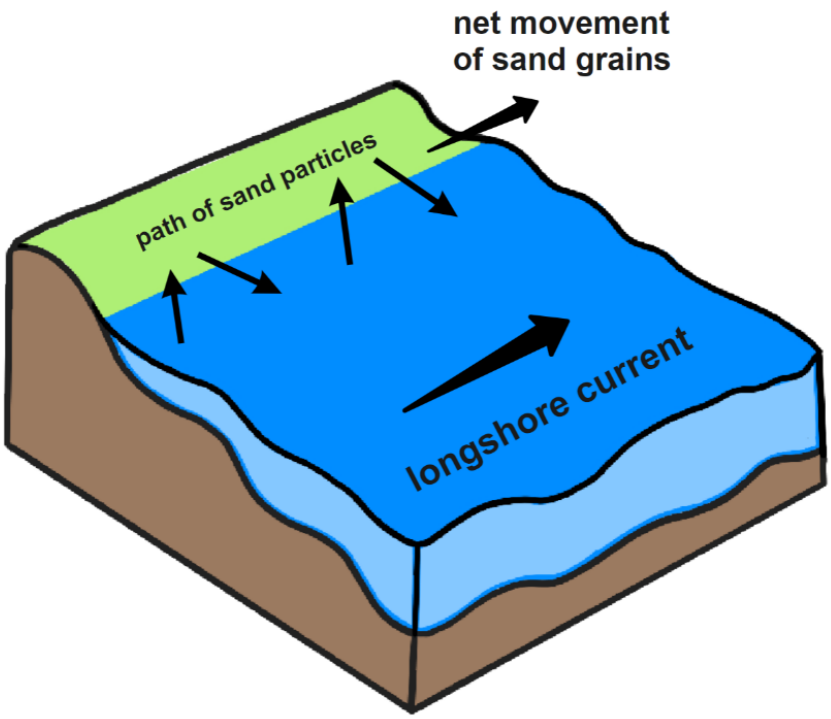

Figure 2.1 The process of Longshore current that moves sand along the beach (Modified from Adelaide's Coastal Erosion, 2015)

Erosion of sandy coasts also has seasonal characteristics. In the season when the waves are flat, the waves deposit sand into berms and wider beach areas. This is because the diagonal current of the waves has enough energy to carry sand to the beach, but the backwash effect is relatively weak, so there is not enough energy to pull the sand away.

This kind of waves is also called constructive waves (Figure2.2). In windy seasons (such as storms), waves have high energy and are destructive waves (Figure2.2). The waves are strong enough to move a large amount of sand, and the strong backwashing effect and weaker scour, results in sand being removed from the beach (Niven & Bardsley, 2012).

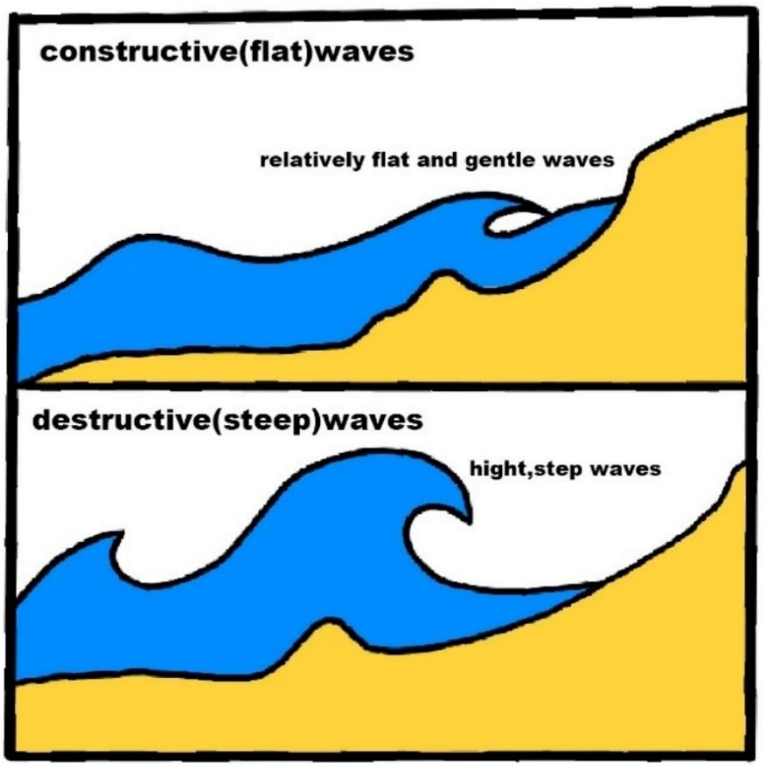

Figure 2.2 Constructive waves and destructive waves (Modified from Adelaide's Coastal Erosion, 2015)

2.2 Coastal Erosion Monitoring

The trend of global population migration is to move closer to coastal areas. At the same time, sea levels continue to rise, and coastlines are constantly being eroded (Stephen et al., 2005). At present, Europe loses about 15km^2 of land due to ocean erosion annually, so buildings in coastal areas are greatly threatened (Rijn,2011). Sweden is one of the northernmost countries in the world, with a total area of around 528000 km^2, and the third-largest country in the European Union (Central Intelligence Agency,2021). The coastline of Kristianstad is approximately 30 kilometres long and contains many different types of coastlines (Erosionsutredning Kristianstad, 2018). Therefore, it is

important to carry out coastal erosion monitoring in Kristianstad.

High-resolution image data and DSMs are widely used to monitor coastline erosion and check the cause of erosion. When monitoring and analyzing coastal changes, it is necessary to continuously collect data for coastal areas. There are several traditional data collection methods: peg-lines, total station, Terrestrial Laser Scanning (TLS), airborne LiDAR (Light Detection and Ranging), Global Navigation Satellite System (GNSS) surveys, and aerial imagery (Clark, 2017). The previous methods can express coastal features for coastal erosion monitoring, but these methods have different accuracy and limitations.

Peg-lines is using pegs for measurement (Figure 2.3). When the distance to be measured is short and the distance to be measured does not exceed the total length of the chain, set nails as markers at the start and endpoints. Then fix the zero point of the chain at the centre of the nail at the starting point and straighten the chain so that the end is fixed at the centre of the nail at the endpoint. The reading of the chain is the distance user want to measure. The advantage of the peg-lines measurement method is that it is easy to establish and perform repeated measurements and the disadvantage is that it is difficult to obtain a large amount of data over larger areas limited (Gulyaev & Buckeridge. 2004). The TLS investigation method may obtain very accurate results, but the data processing time is long, and the investigation process is complicated (Clark, 2017). In addition, the airborne LiDAR survey method can collect data in a large area, but the spatial and vertical accuracy of the results obtained cannot be compared with GNSS and TLS, and the cost is very expensive (Mancini et al. 2013). GNSS is also a fast and accurate survey method, but GNSS is limited by measurement points where elevation is measured. The other is that when performing a large-scale measurement, due to the limitation of the number of equipment, the measurement time of different measurement points will be different, so the measurement point may be affected by tides or other topography. (Clark, 2017).

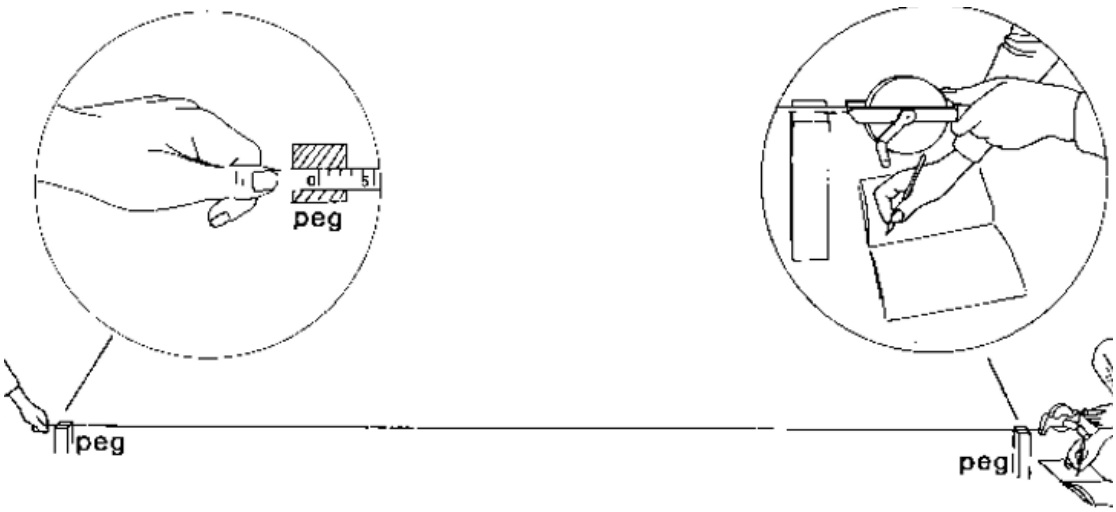

Figure 2.3 The method of peg-lines measurement (Modified from Brouwer, 1985)

By comparing the coastline in the aerial photos captured at different times, the degree of coastal erosion can be analyzed, and the coastal erosion can be monitored but elevation changes are not included, which is a disadvantage to DSMs (Webster, 2012). These traditional collection methods can obtain high-resolution data. Although the accuracy of the monitoring can meet the requirements, the disadvantage is that the cost is high, and it is difficult to carry out long-term multiple coastal erosion monitoring.

2.3 UAV for Erosion Monitoring

The use of traditional measurement methods will be restricted by the topography. For example, the surface shape of the beach is undulating and the shape is easily changed, the setting of many points on the beach will be greatly restricted. Compared to traditional monitoring methods, the use of UAV for images collection is low in cost, easy to operate and has fewer limitations (such as limitation of terrain). Compared with GNSS measurement, UAV measurement only needs to set a few control points, so it is very advantageous for places that are not convenient for surveying personnel to reach. In addition, during UAV measurement, the flight can be completed according to the set height, so it will not be blocked by obstacles such as buildings. UAV enables monitoring

of large areas with higher temporal and spatial resolution. UAV has been used in coastal areas to map river channels (Flener et al. 2013), generate DSM of a beach dune system (Mancini et al. 2013), and investigate aeolian dune formation and evolution (Hugenholtz et al., 2012). UAV has the characteristics of low-cost equipment and a high degree of automation, which makes it advantageous when monitoring coastal erosion. The images obtained by UAV have high spatial resolution and can be measured corresponding to the preset ground control points (GCPs), all these GCPs will be used to help to set DSMs' coordinates system later. The size of a UAV is small, and it is easy to find take-off and landing sites (Gonçalves & Henriques, 2015). When the UAV is flying, the area covered by the camera can usually be viewed in real-time on a screen, and the image area can be checked on-site to ensure that images were captured according to the plan and that they are of sufficient quality. UAV is easy to deploy, so they can be easily implemented when a quick response is required, for example, measurements can be taken immediately after rainfall or a storm. Moreover, because the UAV does not require a pilot to ride, an accident will not cause a loss of personnel.

UAV monitoring also has some disadvantages. Since common UAV uses batteries to provide energy, the battery is the main limitation of a UAV's flying time. The flight time is also affected by natural factors such as wind, and the time and area for each shooting will be limited (BBC, 2015). The distance between the operator and the UAV is also limited. The UAV itself has sensors such as GPS, which can be used to locate the camera position, but usually, these sensors are used for navigation rather than positioning for measurement accuracy.

UAV will also be affected by the flight environment when monitoring coastal erosion. First, meteorological conditions, such as strong winds, will cause problems with the flight and stability of UAV, usually need to choose an environment where the wind speed is lower than 25km/h. The environment also influences the ability to create 3D models of the captured images, for example over large water bodies. The influence of

sea waves and other water bodies is unavoidable in coastal erosion monitoring, and water bodies may make image matching fail. When the data is further processed, Mask can be used to remove the interference in the water body area. Mask mainly extracts the target area from the entire data or masks the noise area such as the water body by selecting the boundary of the target area or the boundary of the water body area (Gonçalves & Henriques, 2015).

2.4 Structure from Motion (SfM)

Using UAV for photogrammetry is a Structure from Motion (SfM) measurement method. SfM is used to perform a 3D reconstruction of the target (e.g., the beach that is monitored) by acquiring multiple images with overlapping regions at different locations in space (Figure2.4). SfM uses a similar method as traditional stereophotogrammetry to continuously take a large number of photos of the same area from different angles and build a 3D model based on the overlapping image parts in many photos. In Figure 2.4, the red and blue lines show the range of ground measurement; i and i' represent the angle between the camera and the vertical direction. SfM is much more flexible when it comes to how the images can be captured but they both capture images along flight tracks.

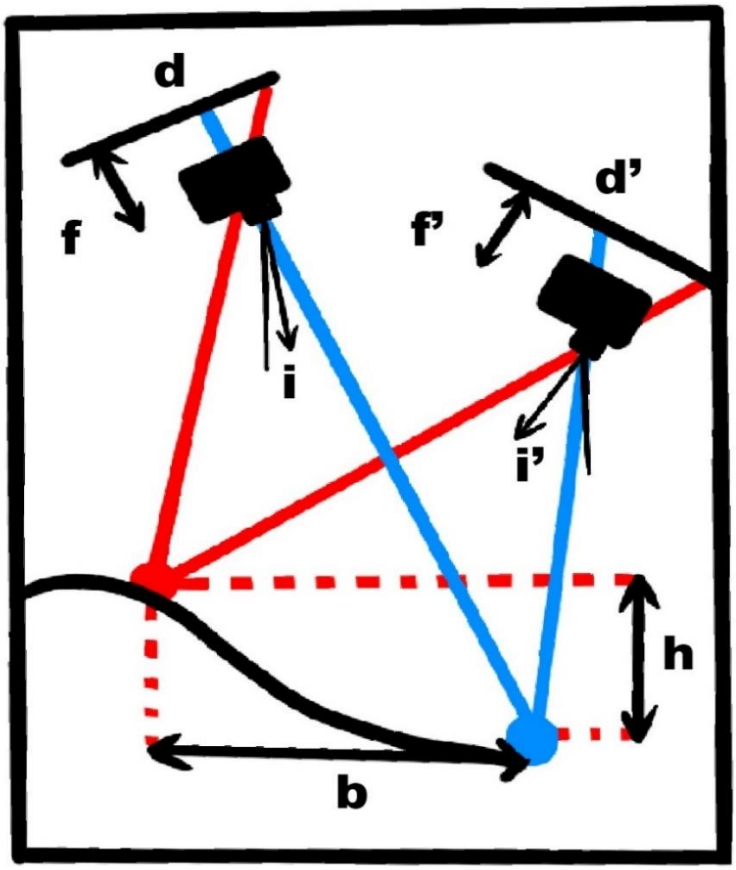

Figure 2.4 Structure from motion (SfM) measurement (Modified from Nissen, 2016)

The workflow of SfM omits the coordinate information of the camera direction and control in traditional photogrammetry and adopts scale-invariant feature detection, which is to find extreme points in the spatial scale. Extreme points are key points, which are points identified in overlapping images and used in the bundle adjustment. According to the location of the extreme points and other parameters, the algorithm detects the local features in the image (SIFT; Lowe, 2004), and least square bundle adjustment algorithm to match between images, align and generate a "Sparse" point cloud that represents the most prominent features (Niamh, Ankit & Mary, 2018). Then the multi-view stereo (SfM-MVS) algorithm (Furukawa et al., 2010) is used to enhance the sparse cloud to generate 3D point clouds and merge them into a single dense point-based model. In general, SfM is to find the feature points in all images through algorithms, align and generate a point cloud, and enhance the point cloud to generate a model based on a single dense point.

On this basis, high-resolution ortho maps, grids and digital elevation models (DEM) can be generated. The image processing software used in this project such as Agisoft Metashape can simply create DSM.

3. Methods

3.1 Study Area

Åhus (Figure3.1) is located on the municipality of Kristianstad's eastern coast, along the Hanö Bay, where the Helge River flows and drains into the Baltic Sea. The downstream catchment area of the Helge River is Sweden's lowest point. This location is 2.41m lower than the average sea level. The most densely populated location along the shore is the city of Åhus. Coastal areas are attractive summer vacation destinations, and their populations will skyrocket throughout the summer. This neighbourhood has between 5000 and 7000 individuals who live in summer cottages along the coast. The biggest hazards to coastal areas are beach erosion and rising sea levels (RISC-KIT, 2021).

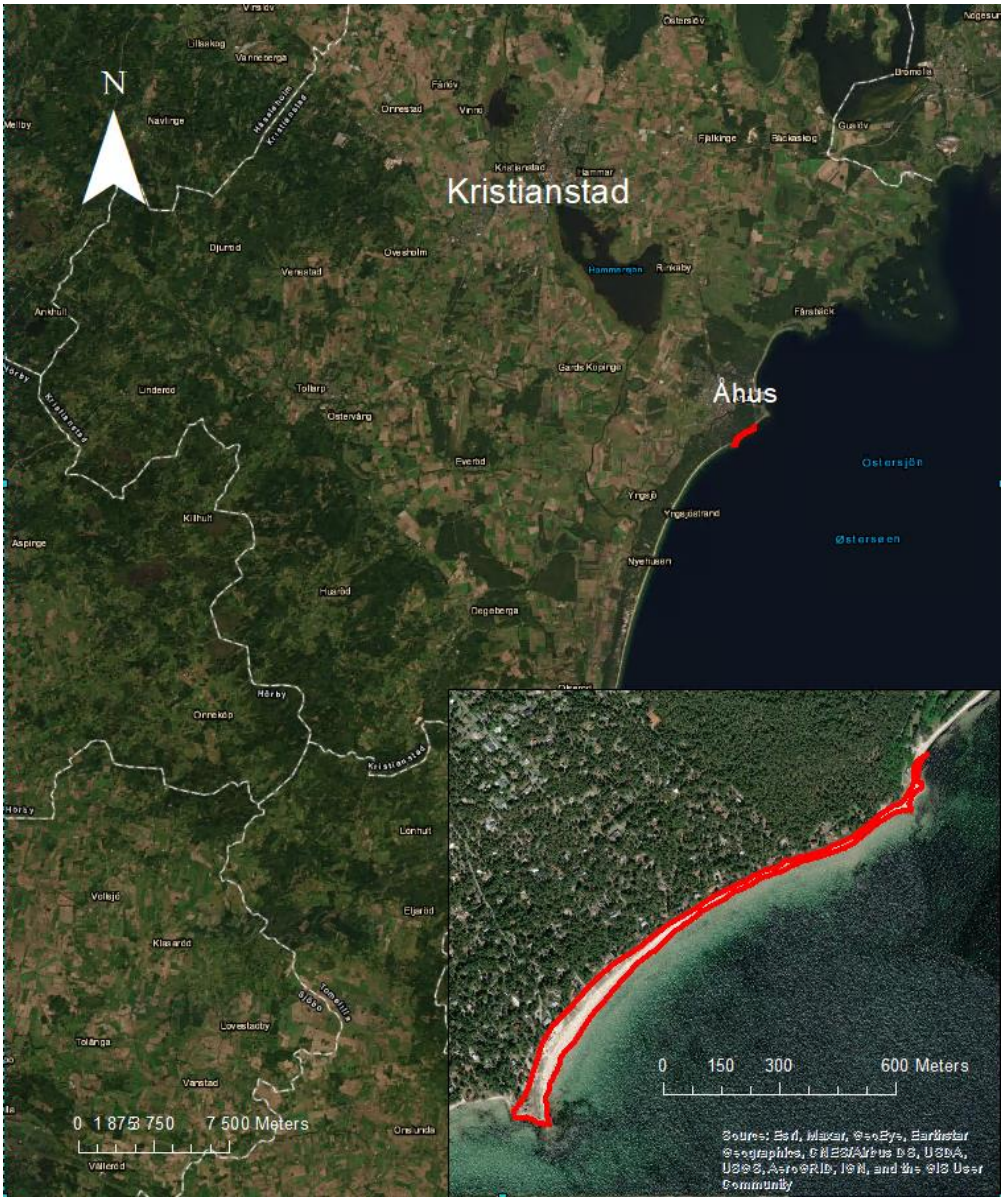

Figure3.1 The municipality of Kristianstads and the study area in Åhus

3.2 Data and equipment

3.2.1 UAV system: aircraft model and camera parameters

The Trimble ZX5 Multirotor UAV (Trimble, California, USA; Figure3.2) and Sony a6000 Camera (Sony, Japan) were used in the project. The relevant detailed specifications are shown in Table 3.1 and Table 3.2.

Figure3.2 Trimble ZX5 Multirotor Unmanned Aircraft

Table3.1 Camera body parameters

Feature	Specification (Sony a6000)
Effective pixels	24.3 megapixels
Image sensor	APS-C 23.5*15.6mm (0.93*0.61”) CMOS
Shutter speed	1/4000-30 seconds
ISO sensitivity	AUTO, ISO 100-25600
Display	7.5 cm (3.0”)tilting LCD monitor
Dimensions(Width*Height*Depth)	120*67*45 mm (4.7*2.6*1.8”)
Weight(body only)	344g

Table3.2 Trimble ZX5 Multirotor Unmanned Aircraft System

Hardware	Type	Rotary wing
	Number of rotors	6
	Maximum takeoff mass	5 kg
	Payload capability	2.3 kg
	Dimensions	85 cm*49 cm
	Material	Carbon frame structure
	Propulsion	Electric pusher propeller;6 bruless motors
	Battery	2*6600 mAh,14.8V
Operation	Endurance	20 minutes
	Maximum celling	3000 m
	Pre-flight system setup time	5 minutes
	Launch and recovery	Vertical takeoff and landing
	Weather limit	Stable in winds up to 36km/h
	Communication and control range	Up to 2 km
Acquisition performance	Resolution (GSD)	1.0 mm to 19.5 cm, depending on height above ground level and lens
	Flight above ground level (AGL) range	5m to 750m

3.2.2 UAV flights

This project's UAV flights took place in 2017, 2019, and 2020. (Table 3.3). Flights in 2017 were centred in October and autumn; flights in 2019 were divided into two seasons: spring in April and winter in December. Flights in 2020 were similarly mostly distributed during two seasons: spring in March and spring in May.

Wind conditions have a significant impact on UAVs and waves, therefore the weather is a crucial issue to consider. Weather data was not collected during the flights but was obtained later from Kristianstad airport (about 10 kilometres east of the beach) for the days of flying.

Table3.3 Flights list and weather (N=north, W=west, S=south, E=east.)

Date	Time	Wind direction	Wind Speed（m/s）	weather
2017-10-10	10:00	WNW	4	Sunny
2017-10-11	11:00	WSW	3	Scattered clouds
2019-04-01	11:00	E	3	Sunny
2019-04-09	11:00	NE	4	Clouds with sunny spots
2019-12-03	11:00	SW	3	Cloudy
2019-12-04	11:00	W	4	Cloudy
2020-03-23	11:00	S	4	Sunny
2020-03-25	11:00	SW	3	Sunny
2020-05-28	11:00	NE	3	Sunny
2020-05-29	11:00	NE	3	Sunny

3.2.3 Ground control points

Ground Control Points (GCPs) were employed as the foundation of UAV image georeferencing in this research, which are the control points that properly measure the coordinates and elevation using total station and GNSS. Two GCP styles were primarily employed. One is a white square point, and the other is a yellow and black rectangular ground control point, as seen in Figure 3.3. The GCPs must be evenly distributed in the research area by the staff before the UAV flight. Real-Time Kinematics was used to determine the positions of all control points (RTK). The SWEREF99 13 30 coordinate system was used to measure the GCPs (EPSG: 3006).

Figure3.3 The two styles of GCPs used for the flights

3.3 Data processing and analysis

In this study, UAV photos were used as data input, and UAV photos were processed using SfM to create DSM, Orthomosaic, and other data sets. ArcMap was used to produce additional maps and analyse the generated DSMs (Figure 3.4).

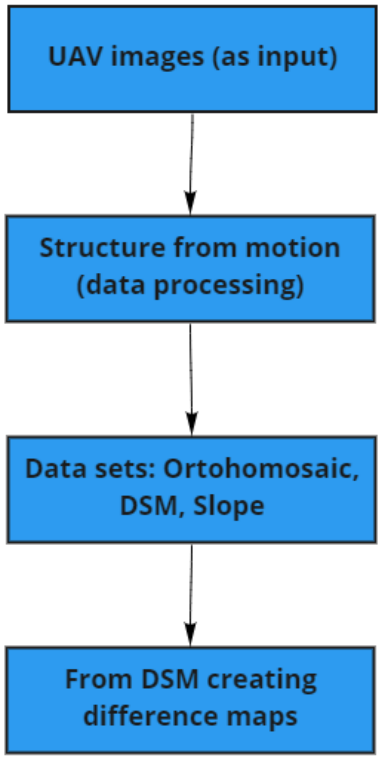

Figure3.4The general workflow of the data processing

3.3.1 DSM generation from UAV data

This stage was primarily concerned with processing the collected UAV image data in order to produce a high-quality DSM. DSM is the end outcome of this study. Because the beach has no vegetative cover, the elevation related to DSM in this project indicates the elevation of the beach. Due to time constraints, the Align photo process utilised the High standard, while the Build Dense Cloud procedure utilised the Medium standard. Figure3.5 depicts the full operation steps.

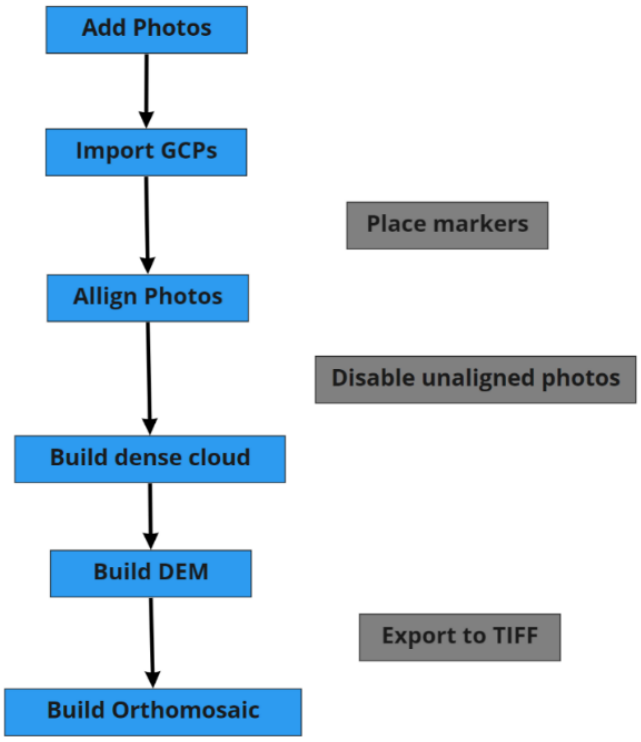

Figure3.5 The workflow of DSM generation

It aligns pictures, builds dense cloud, builds DSM, and builds Orthomosaic photo in Agisoft Metashape (Agisoft LLC, St. Petersburg, Russia). Because the pictures did not provide geographic coordinates, georeferencing was conducted on the UAV photographs that included GCPs after importing all of them and constructing the sparse point cloud. The primary approach for georeferencing photographs was to manually find and label GCPs on the map, as well as mark GCPs in each photo after importing GCP position information. Markers should be placed in the figure. Align all of the

photos after you've finished marking the GCPs. GCPs Accuracy was set to 0.05m during this operation, and the coordinate system was set to SWEREF99 13 30. (EPSG: 3008). During the aligning process, the GCP accuracy value cannot be too high. The Align will be limited if the precision is too great. The photo stitching method resulted in displacement and distortion of the findings.

3.3.2 DSM quality assessment

The quality requirements of the DSM were mainly reflected in two aspects: horizontal and vertical accuracy. The error of the horizontal accuracy was the difference between the DSM and the actual horizontal position of the same point. In the process of data processing, the error in the horizontal direction might come from the error in the selection of GCPs, the error in UAV image Align, etc., The errors in the horizontal direction of all GCPs measurement values and GCPs in DSM can be displayed in Agisoft Metashape. The average tolerance is 0.05 m. The horizontal accuracy can also be verified by orthomosaic. After creating and exporting DSM and orthomosaic in Agisoft Metashape, opening the output result in ArcMap and importing GCPs with SWEREF99 13 30 (EPSG: 3008) projected system into ArcMap. To verify the horizontal accuracy of DSM by comparing the deviation of the orthomosaic and GCPs measurement positions under the unified coordinate system, exporting orthomosaic and GCPs need to be overlapped. In a generally flat area like most of the beach, the horizontal error will not have a large influence on the vertical error compared to hilly areas.

The elevation is the most important data in this project, so vertical accuracy is also very important. First of all, the z-error limitation in Agisoft Metashape, that is, the error and average error of all GCPs in DSM cannot exceed 0.5. Accuracy maps were created in ArcMap according to each DSM to display the different error range of each GCPs as a reference for analyzing the differences of elevation in the study area. The accuracy maps were created by calculating the difference between the measured value of the

GCPs and the elevation for that point in the DSM.

3.3.3 DSMs differences calculation

The coastal erosion was quantified by changes in elevation in DSM from two different times. The change of beach was calculated according to Equation 3. 1 with the Raster Calculator in ArcMap.

$$Elevation_{change} = E_{year1} - E_{year2} + ERROR_{year1} - ERROR_{year2} \quad \text{(Equation 3.1)}$$

E_{year1} is the elevation from the end year, E_{year2} is the elevation from the start year. $ERROR_{year1}$ and $ERROR_{year2}$ are the error from these years. Since the error of elevation can only be estimated at the GCP, it was impossible to obtain the accuracy of each pixel in the DSM. Therefore, when the elevation change area is quantitatively analyzed, the elevation of the nearby GCPs was selected for reference according to the area.
The error of GCPs was obtained by calculating the difference between the measured value and the actual value in the DSM according to Equation 3.2.

$$ERROR = Elevation_{true} - ERROR_{sample} \quad \text{(Equation 3.2)}$$

where $Elevation_{true}$ is the elevation value from RTK, $ERROR_{sample}$ is the elevation value sampling from DSM. Since the measured value Elevation true is measured by RTK, it is considered as the true value. After the DSM is created by Agisoft Metashape. Then import DSM into ArcMap, and the Sample function is used to obtain the value represented by each GCP in DSM.

3.3.4 Slope Map

Slope maps were also created in this project. Slope map is mainly created in ArcMap, through Slope processing of DSM. For each pixel, the slope (Figure 3.6) in ArcMap is calculated from the maximum rate of change from that pixel to its neighbouring pixels

(Burrough & McDonell, 1998). The lower the slope value, the flatter the terrain; the higher the slope value, the steeper the terrain. The distribution and severity of coastal erosion can be understood by analyzing the difference in slope. Per cent of the slope is calculated according to Equation 3.3.

$$\text{Percent of slope} = \text{rise/run} * 100 \quad \text{(Equation 3.3)}$$

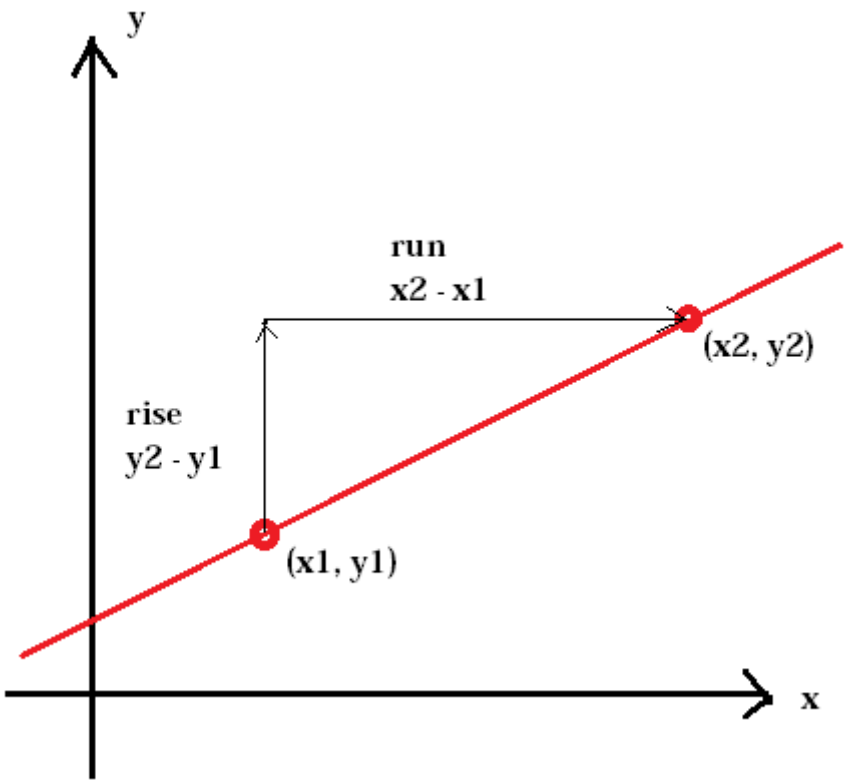

Figure3.6 The slope of a linear function

3.3.5 Mask of the study area

In this project, the UAV image not only contains the beach in the study area but also contains a large amount of irrelevant information such as water area, trees and buildings (Figure 3.7). The profile created by the dense cloud (Figure 3.8), shows that the noise of the water body on the right is obvious, in contrast to the smooth beach. In DSMs, the water body was very large and full of noise, which is of no significance to the study of beach erosion; there was also a lot of noise at the edge of DSMs, where there was not

sufficient overlap between images, and the changes of buildings and trees outside the beach were not the scope of this project. Therefore, after the DSMs were obtained, a shapefile of the study area (Figure3.9) was created in all DSMs, and the beach area of the study area was selected from the entire DSM using this as a mask, and the noise of the water body, trees, buildings, etc. was removed.

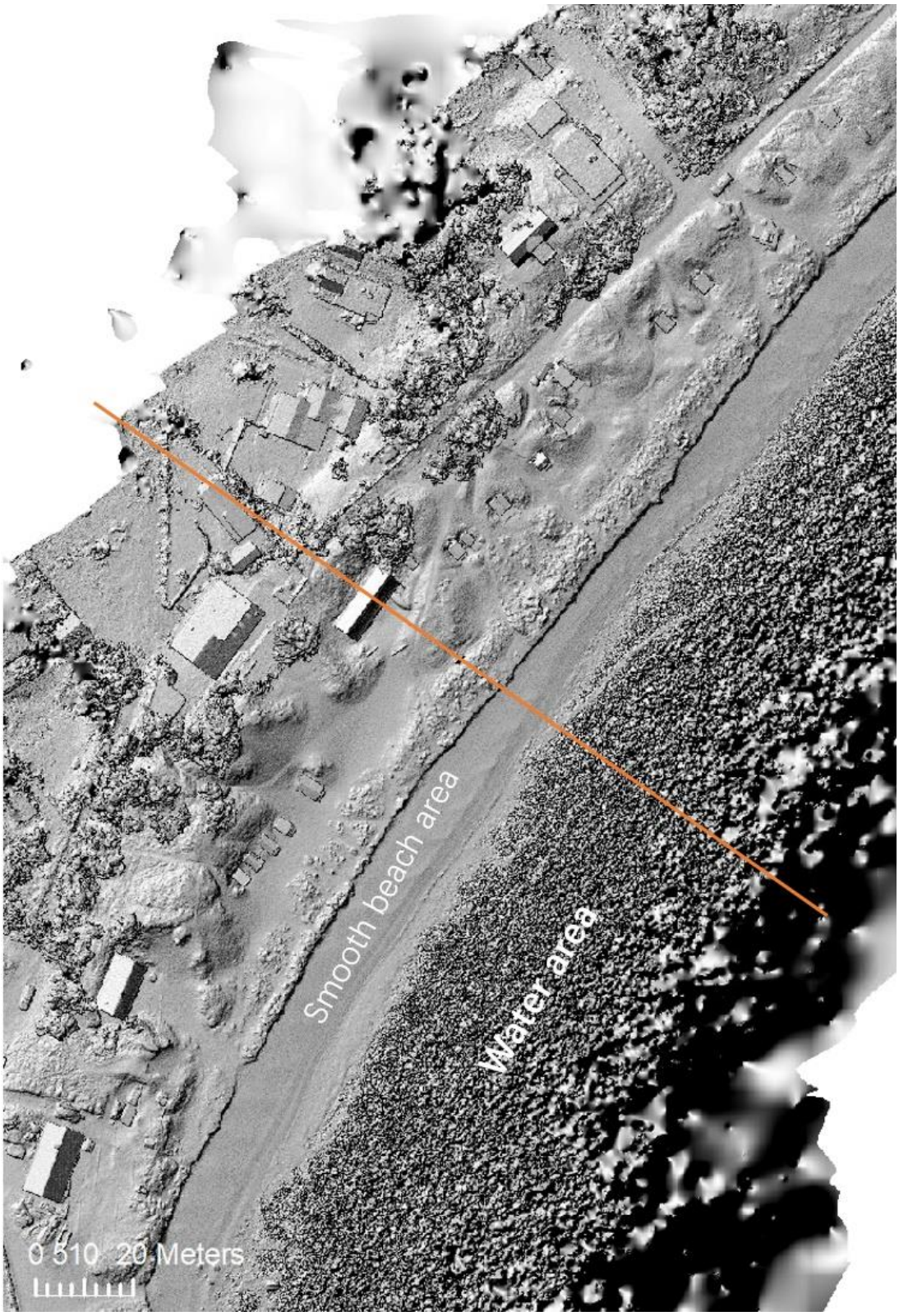

Figure3.7 Hillshaded DSM with water noise and smooth beach area. Approved for publication (spridningstillstånd), LM2021/020180.

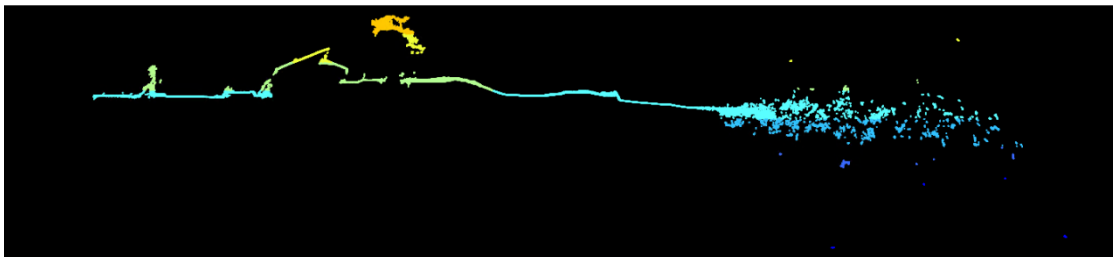

Figure3.8 Profile of water noise (right), smooth beach area and buildings. etc along the orange line

Figure3.9 Mask area in orthomosaic. Approved for publication (spridningstillstånd), LM2021/020180.

Since the scour range of the seawater to the sandy beach is dynamic, the orthomosaic photo created when determining the seawater area can directly and accurately determine the extent of the study area. The area in the red frame in Figure 3.9 was part of the research area of this project.

4. Results

The results mainly include DSMs, Orthomosaic photo, DSM accuracy maps of the study area, beach elevation difference maps of the study area, and beach slope maps of the study area.

4.1 Beach Hillshaded DSM

Figure4.1 shows the hill shaded DSM of March 2020. The hillshade processing of DSM is done to visually enhance the details in the topography of the beach, but the unprocessed DSM is still used in the quantitative analysis of beach erosion. It can be seen from the figure4.1 that the DSM created in Agisoft Metashape contains a lot of noise. The noise is mainly present in two parts, one is the water body, which is mainly distributed on the southeast side of the map; the other is the border area of buildings, trees and drone images. The main research area in this project is the sandy beach, which is the area from the sea to the vegetation coverage area. Therefore, noise from seawater and buildings will be removed by mask.

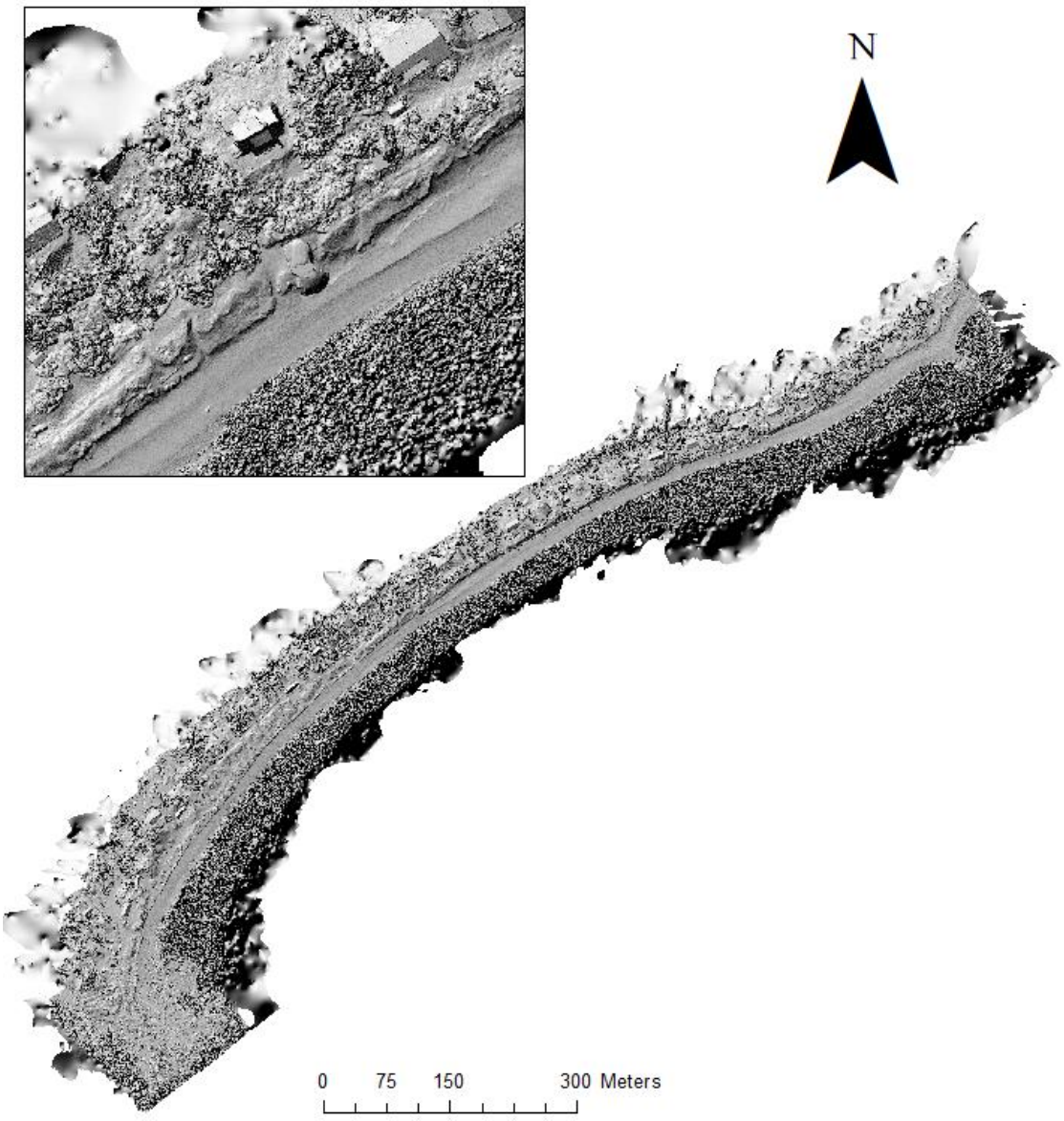

Figure4.1 Hillshaded DSM of March 2020. Approved for publication (spridningstillstånd), LM2021/020180.

4.2 Beach Orthomosaic

Figure4.2 shows the orthomosaic and boundary of the study area. the orthomosaic created in Agisoft Metashape in March 2020. This orthomosaic photo mainly shows different features on the ground and areas of seawater. The area selected by the red line is the research area in this project. This area was manually selected in the orthomosaics in different years because the UAV image of each DSM was taken at a different time and the range of waves on the beach was different. The southwestern part of the coast

contains a wider area because the terrain of this area is relatively flat, with less tree coverage, which may be more affected by the sea; the opposite is the study area in the central and northeastern part of the coast is relatively long and narrow. It is believed that this area is covered with more trees and has obvious topography.

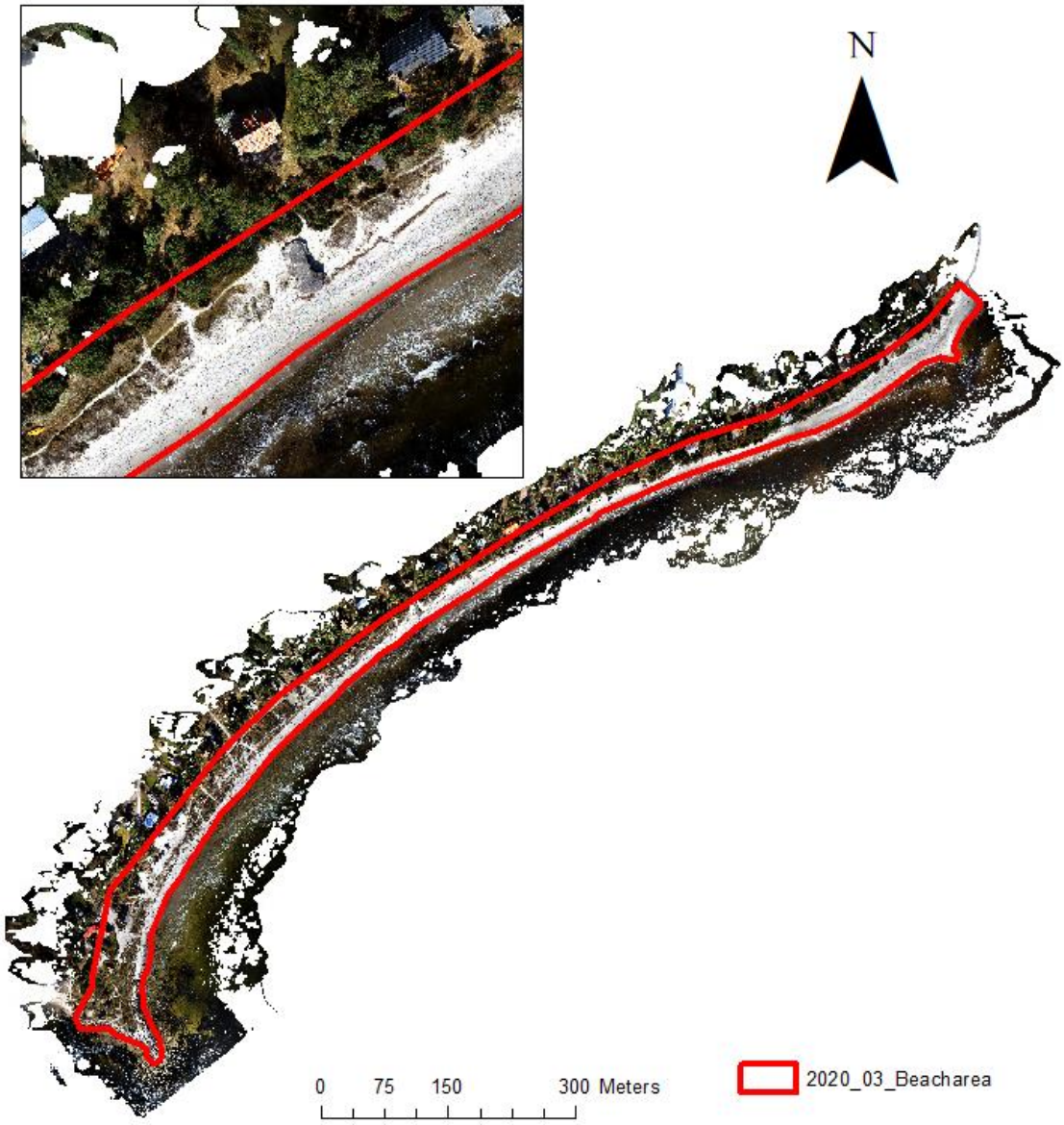

Figure4.2 March 2020 Orthomosaic photo and boundary of the study area. Approved for publication (spridningstillstånd), LM2021/020180.

4.3 Beach Elevation differences and DSMs accuracy

In total five DSMs were created, including October 2017, April 2019, December 2019,

March 2020 and May 2020 and four difference maps were created. Table 4.1 lists, the difference maps, including names and equations used to create the maps.

Table4.1 Table of difference maps and equation used to calculate the difference maps

Name of difference maps	Start date	End date	Calculate equation
2005_2003_bea	03/2020	05/2020	05/2020 – 03/2020
1912_1904_bea	04/2019	12/2019	12/2019 – 04/2019
1912_1710_bea	10/2017	12/2019	12/2019 – 10/2017
2003_1904_bea	04/2019	03/2020	03/2020 – 04/2019

The difference in ground elevation between two DSMs is used to calculate beach erosion. Elevation differences of 0.3 m were used to classify the difference maps. Because the greatest error value derived from the accuracy map in the same year is 0.3 m, choosing 0.3 m as the classification interval may effectively identify the genuine change from the impact of the mistake. The Elevation result uses yellow, light green, green, dark green, and so on to show negative values, indicating that the elevation of these areas has increased during this period. The outcome, on the other hand, employs orange, red, and dark red to signify positive numbers, implying that the elevation of these areas is reduced. In the accuracy maps, red and other colours reflect negative values, indicating that the DSM's elevation is greater than the measured elevation at the GCP. Green and other positive values indicate that the DSM at this site is lower than the measured elevation at the GCP.

4.3.1 Elevation differences between 05/2020 & 03/2020

Differences in Elevation between 05/2020 and 03/2020 are shown in Figure4.3. It is found that most of the differences in the beach area are classified as yellow, dark yellow and orange (i.e. positive differences) in individual areas. The orange areas are mainly distributed in the middle of the beach and a small part of the southeast of the beach. Comparing the DSM accuracy maps of the past two times (Figure4.4 & Figure4.5), in the northeast of the beach, the accuracy of 03/2020 is relatively high. The error is in the range of - 0.05 – 0.05 m and the average is about 0.01 m; the error of 05/2020 fluctuates

greatly. Approximately in the range of -0.2 – 0 m, the average value is about - 0.1 m. Because the positive and negative values of error are different, the disturbance direction representing the error is different, so the absolute value of the average error in the northeast of the beach is about 0.11 m. In the middle of the beach, the accuracy of 03/2020 is relatively high. The error is in the range of - 0.05 – 0.05 m and the average is about 0.03 m; the error of 05/2020 fluctuates greatly, about - 0.2 – 0.2 m, the average value is about - 0.06 m. Because the positive and negative values of error are different, the disturbance direction representing the error is different, so the absolute value of the average error in the northeast of the beach is about 0.06 m. In the southern part of the beach, the error of 03/2020 is in the range of - 0.13 – 0.15 m and the average is about 0.05 m; the error of 05/2020 fluctuates greatly, and the average is 0.04 m in the range of -0.15 – 0.15 m. Because the value of error is all positive, the disturbance direction of the error is the same, so the absolute value of the average error in the northeast of the beach is about 0.01 m.

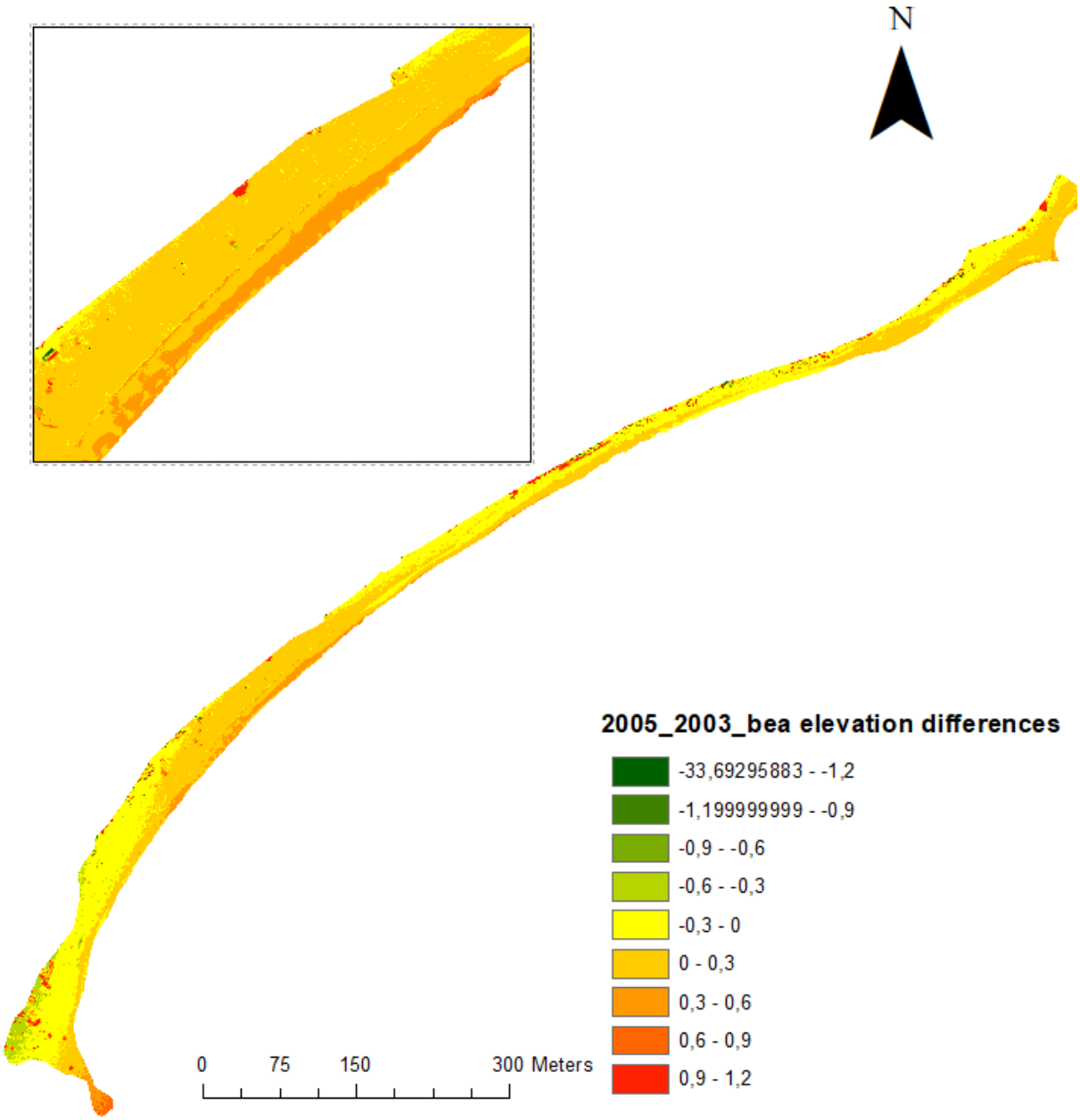

Figure4.3 Elevation difference from March 2020 to May 2020

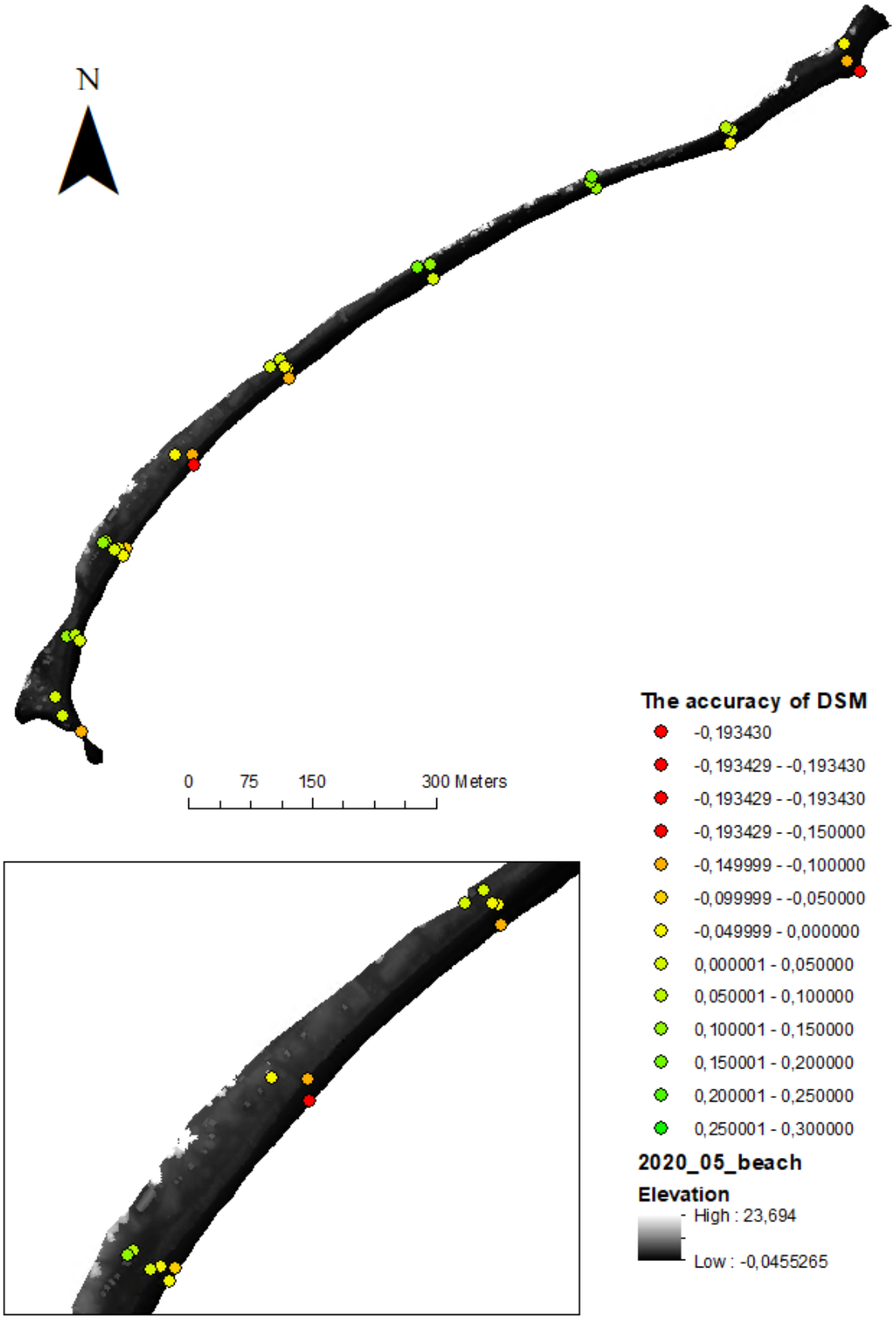

Figure4.4 March 2020 DSM Accuracy at the GCPs

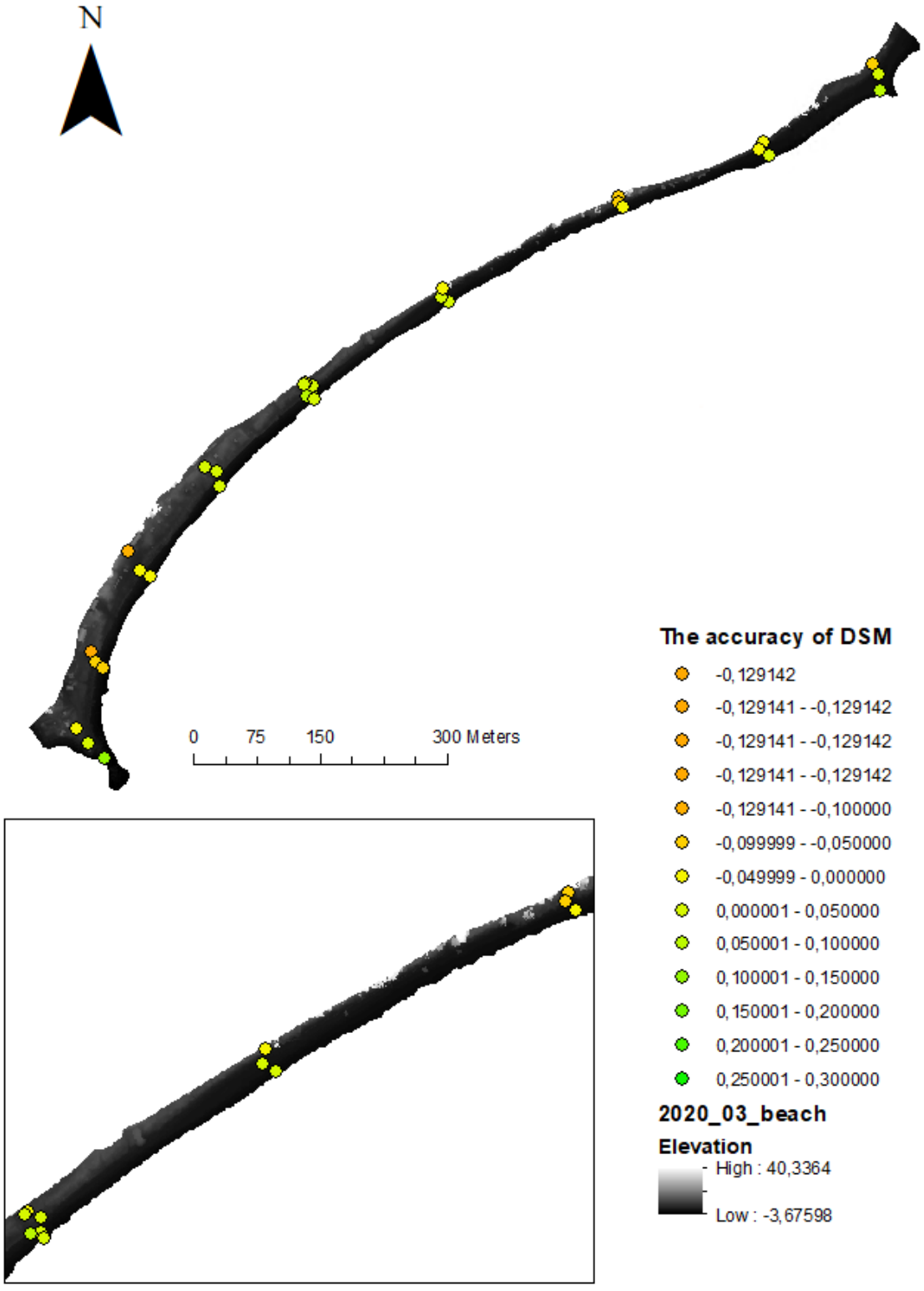

Figure4.5 May 2020 DSM Accuracy at the GCPs

4.3.2 Elevation differences between 12/2019 & 04/2019

The difference trend of elevation is relatively concentrated from April 2019 to December 2019. It can be seen from Figure 4.6 that the sandy beaches in the central and northernmost areas are still mainly yellow and dark yellow, indicating that the elevation of sandy beaches has not changed much. In the north-central area, there is a large area of dark green, which means that this area has added 0.6 – 0.9 m of sand during the period from April to December. In this difference map, the impact of error also needs to consider, so the accurate map of DSMs (Figure 4.7 & Figure 4.8) need to be referred to. In the area with large differences in the northern part of the beach, it can be seen from the accuracy map that the error of 04/2019 is also large, about - 0.32 m. The error of 12/2019 is about 0.065 m. Therefore, the average absolute value of error in this area should be 0.385 m.

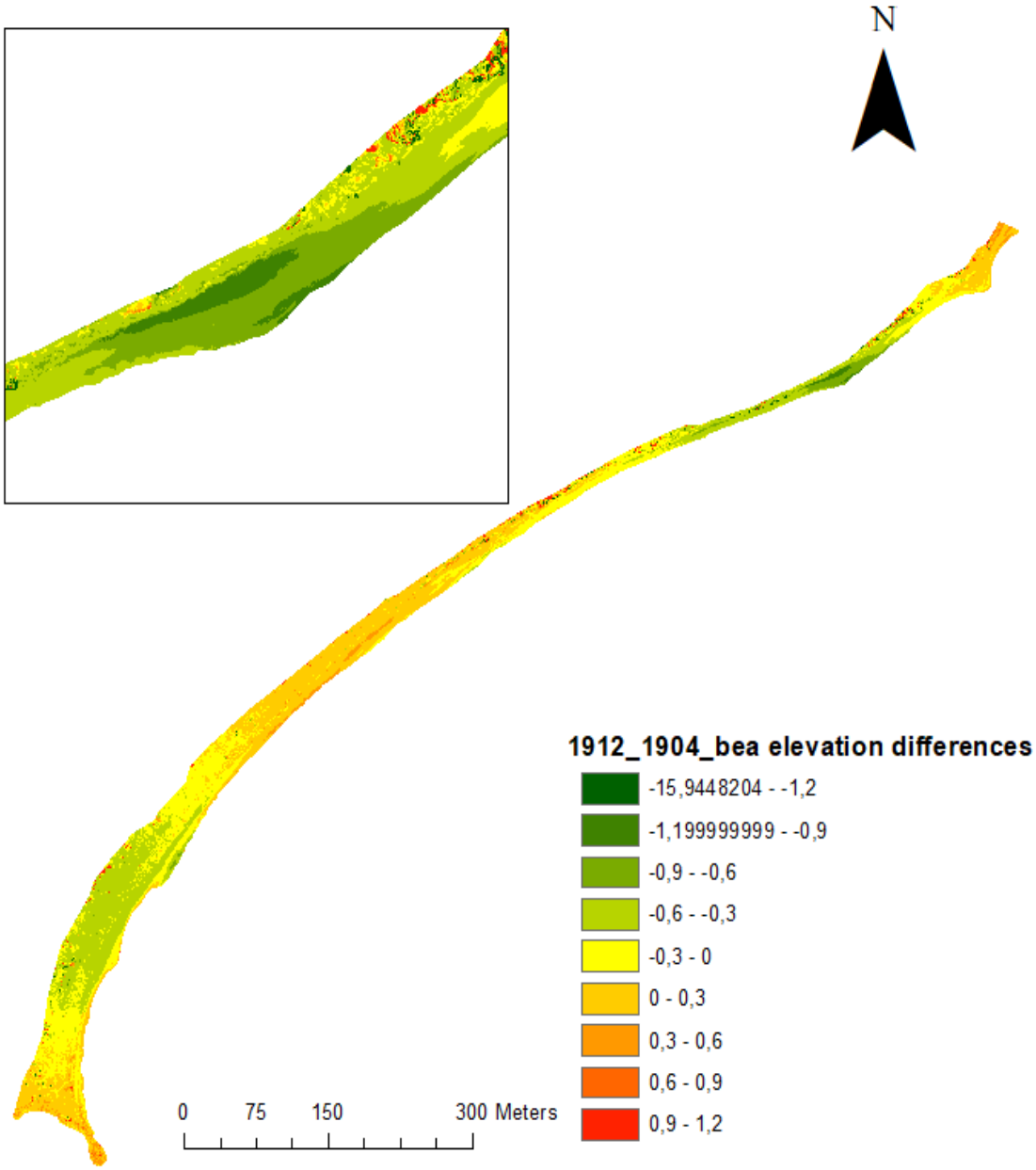

Figure4.6 Elevation difference from December 2019 to April 2019

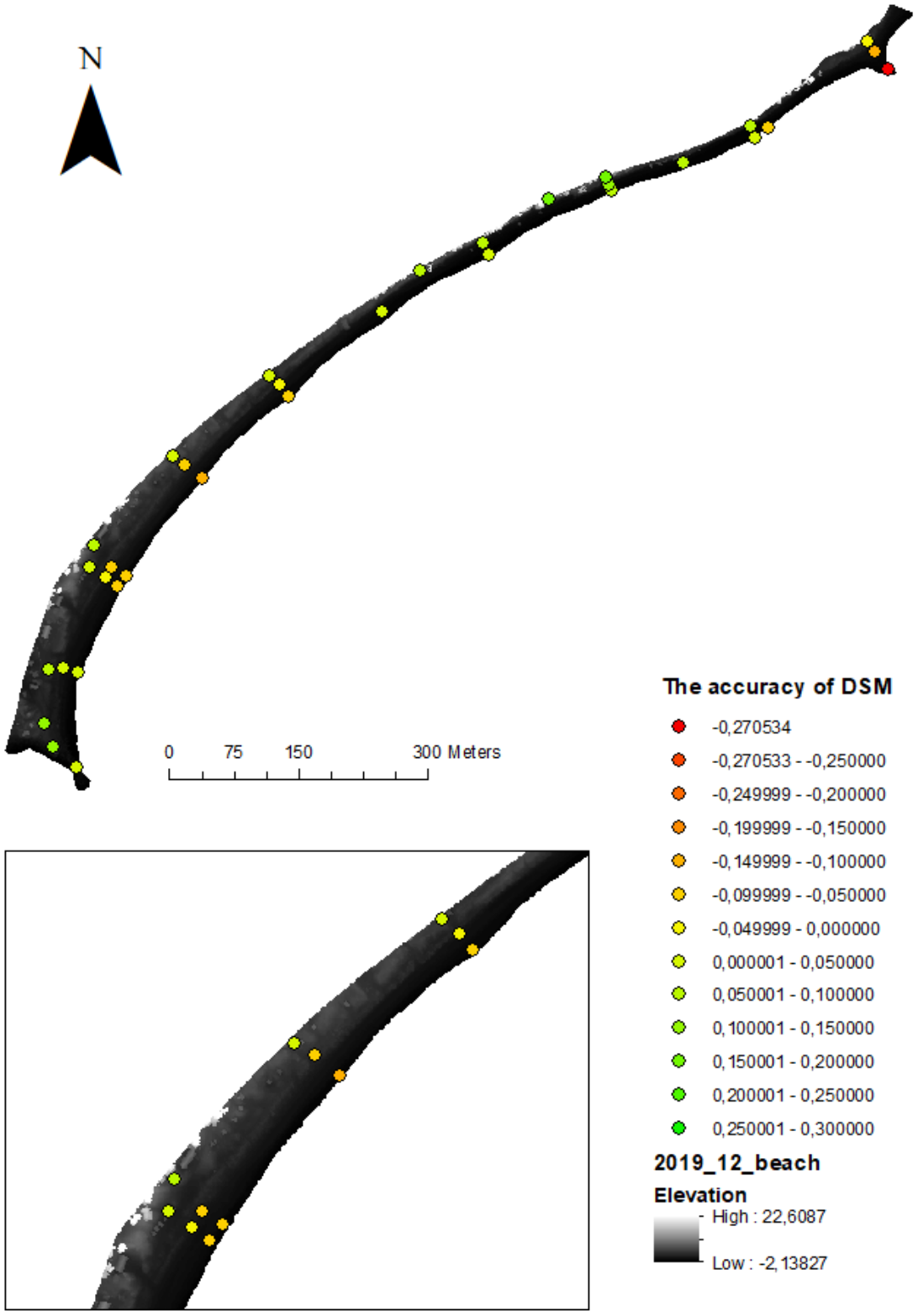

Figure4.7 December 2019 DSM Accuracy at the GCPs

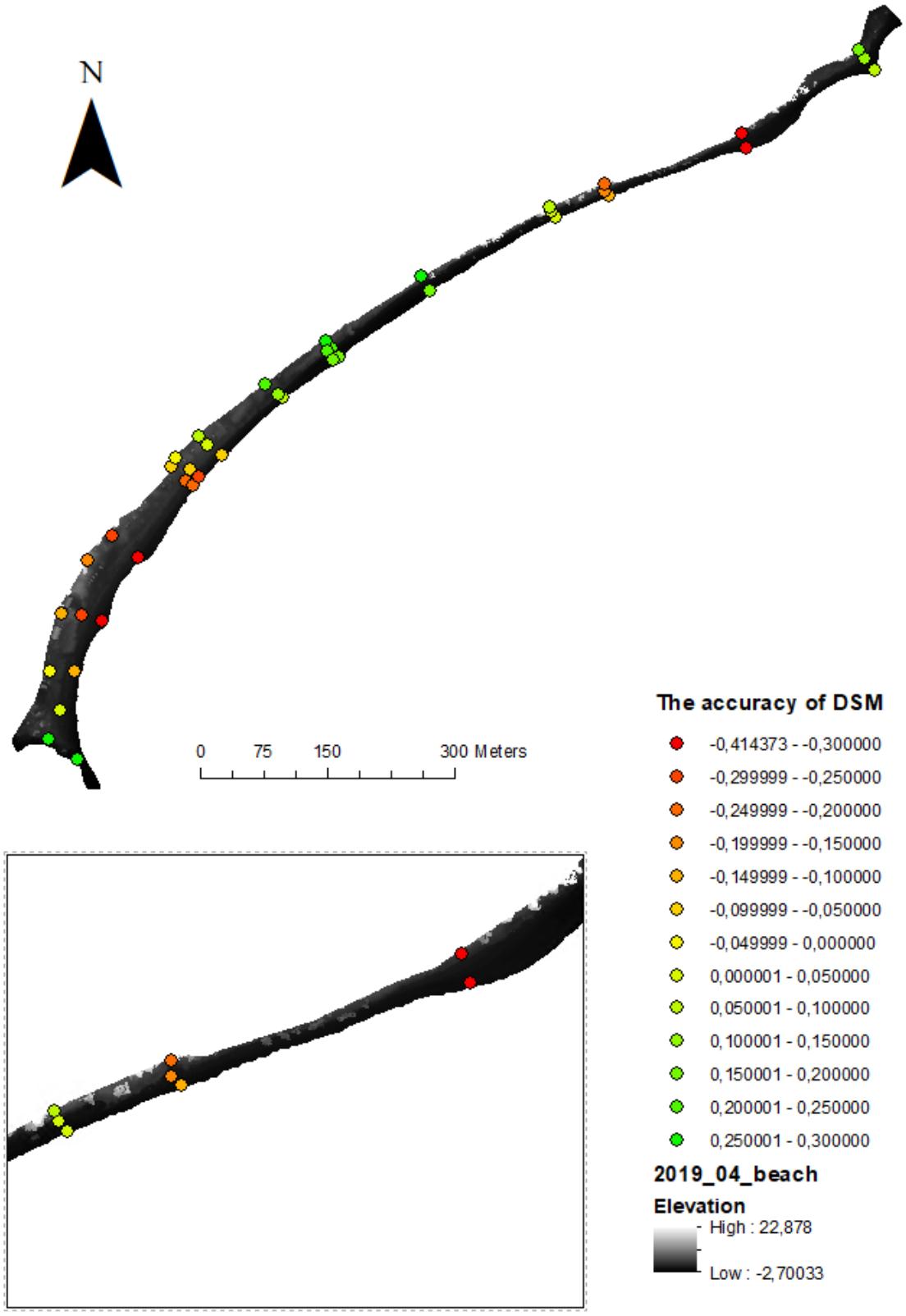

Figure4.8 April 2019 DSM Accuracy at the GCPs

4.3.3 Elevation differences between 12/2019 & 10/2017

The time interval between 12/2019-10/2017 is relatively long, but the overall elevation difference is not particularly strong (Figure4.9). In general, most areas are yellow, and only a small part of the southern and northern areas are bright green and green. According to the 10/2017 accuracy map (Figure4.10), the average error in the northern part of the beach is about - 0.21 m, the average error in the middle part of the beach is about - 0.15 m, and the average error in the southern part of the beach is about 0.2 m. In 12/2019 accuracy map (Figure4.7), the average error in the northern part of the beach is about 0.065 m, the average error in the middle part of the beach is about 0.08 m, and the average error in the southern part of the beach is about 0.07 m. Therefore, the average absolute value of error in the middle area should be 0.23 m.

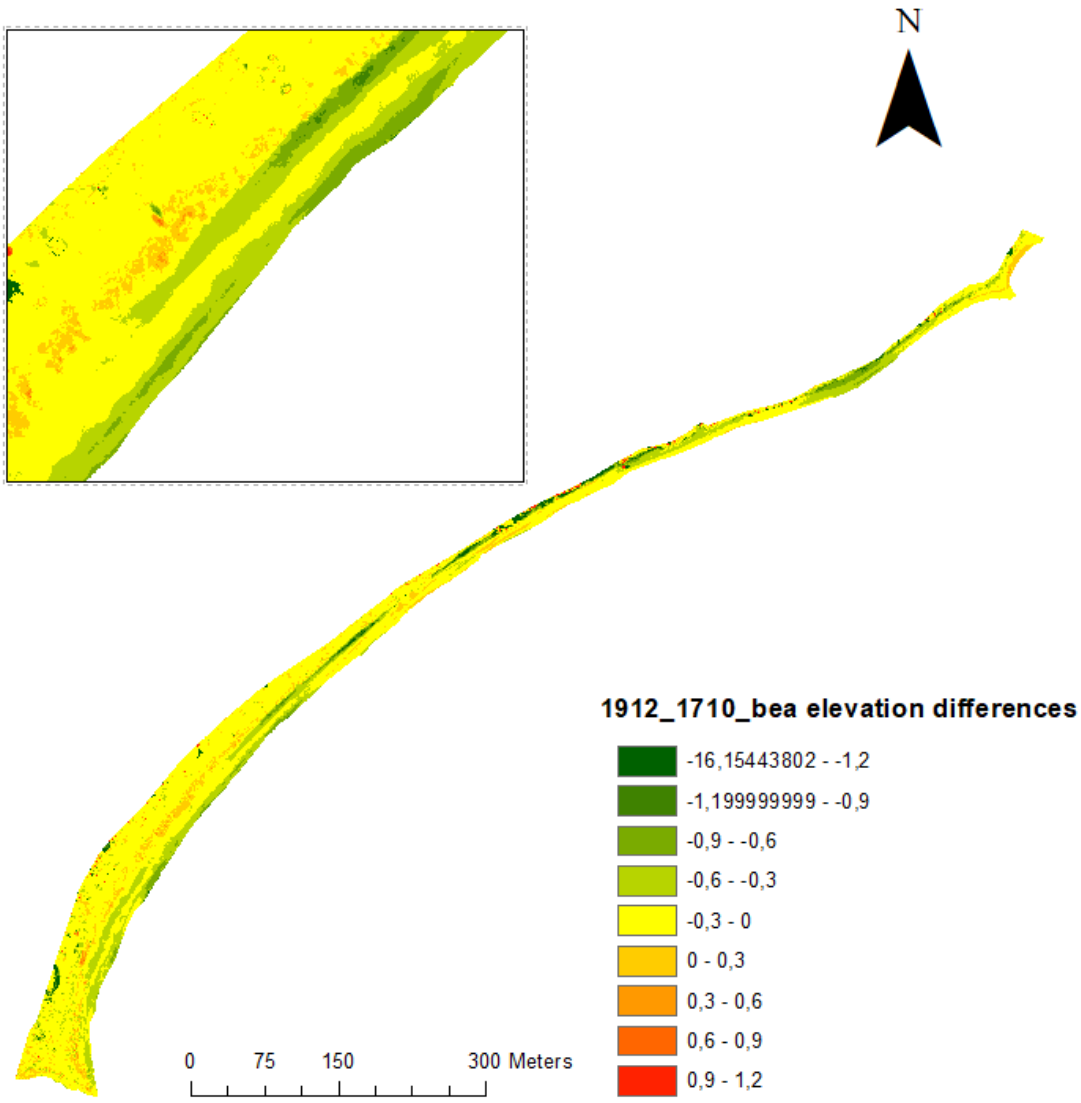

Figure4.9 Elevation differences from October 2017 to December 2019

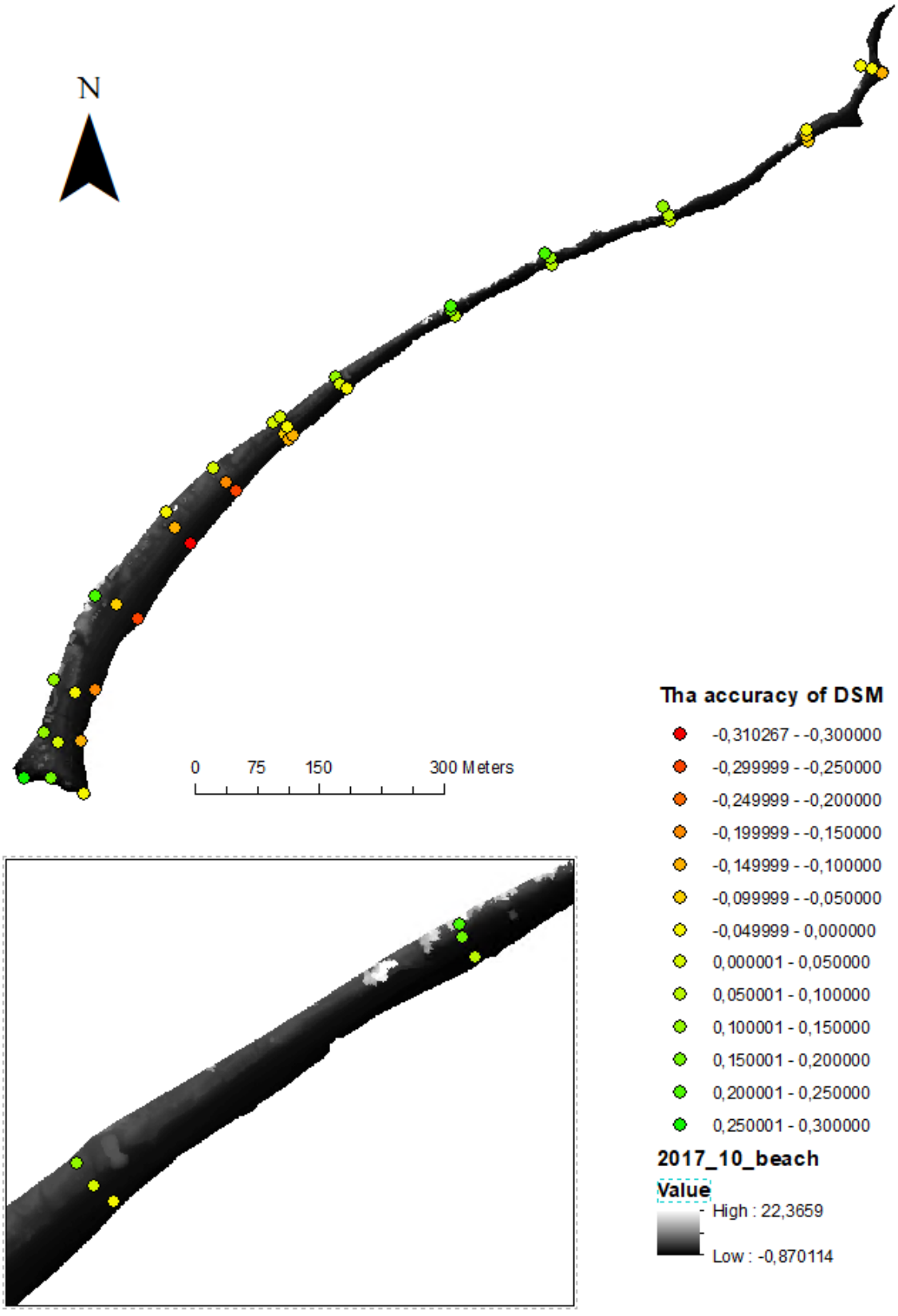

Figure4.10 October 2017 DSM Accuracy at the GCPs

4.3.4 Elevation differences between 03/2020 & 04/2019

The elevation changes between 03/2020 and 04/2019 are more visible (Figure4.11), appearing in most sections of the beach, but the magnitude of the difference is not significant. It features positive values at the top, bottom, and centre, as well as two portions with low values in the middle. The figure shows that the classification of difference is primarily light green in the southern section of the beach, indicating that the beach has lost sand during this period. And the orange and space in the photograph are in the midst of the beach. The majority of the region in this area is orange, with a minor portion of the area classed as red, indicating that this area received a certain quantity of sandy material. There are two tendencies on the northern half of the beach. On the northernmost beach, there is a long strip of crimson, with a pale green region under it. The average error in the northern portion of the beach is around -0.28 m, the average error in the central portion of the beach is approximately 0.15 m, and the average error in the southern part of the beach is around - 0.34 m, according to the accuracy map.

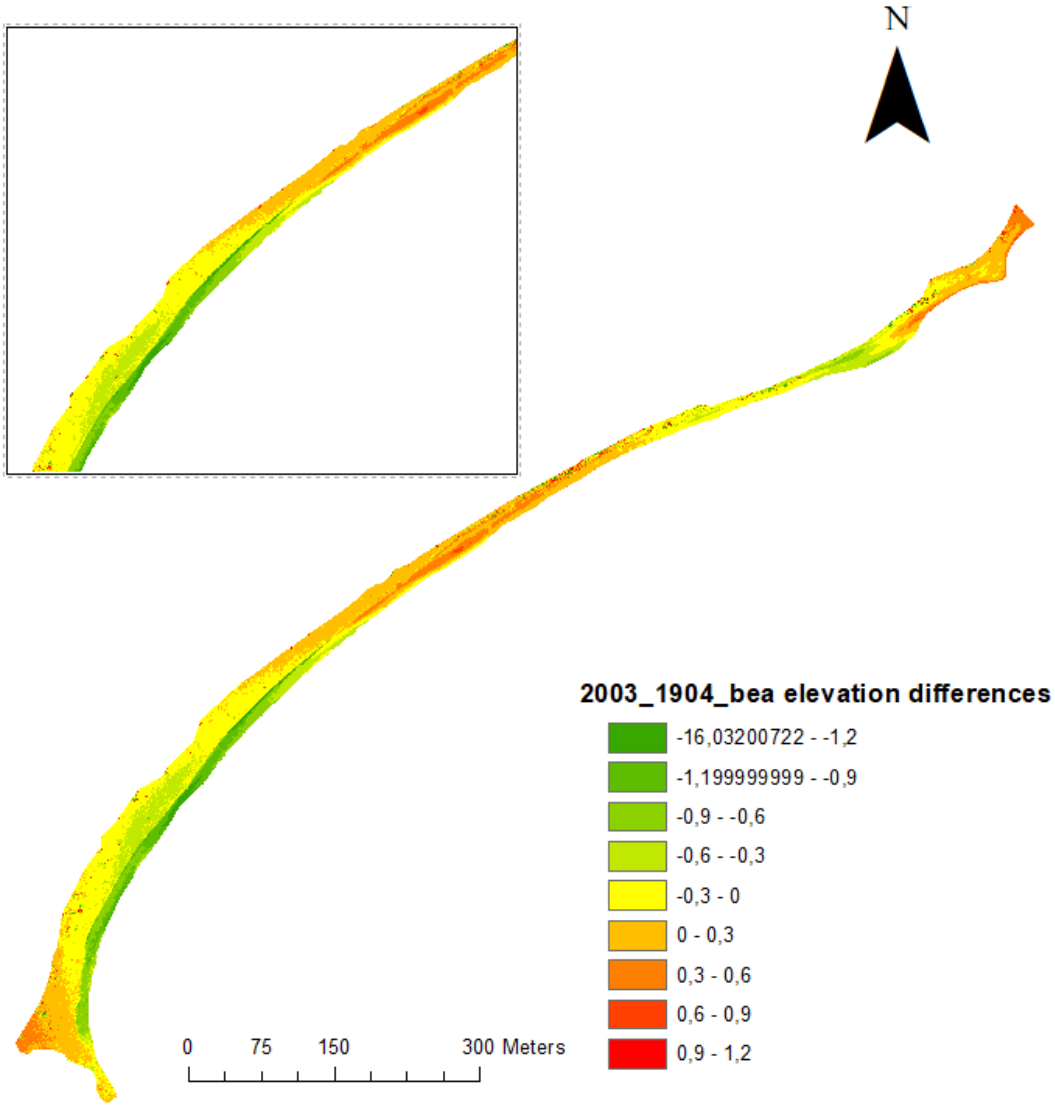

Figure.4.11 Elevation differences from April 2019 to March 2020

4.3.5 Seasonal differences

The seasonal difference can be obtained from Figure 4.6. The seasonal difference is done by comparing two DSMs in different seasons of the same year. It can be seen from Figure 4.6 that in the northern area, a part of it is green and dark green, which means that the beach in this area loses sandy sediment from spring to winter. In the northernmost, central and southernmost parts of the beach, you can see from the map that these areas are orange, which means that these areas get sand from the ocean. Compared with other elevation changes maps, the seasonal difference is not strong

overall, but in some areas, such as the green area in the north of Figure 4.6, the seasonal difference is obvious.

Figure 4.3 shows a short-term seasonal difference, a change from spring to summer. It can be seen from the figure that the changing trend of beach elevation is mainly to obtain sediment from the ocean.

4.4 Beach slope

The slope map from March 2020 is shown in Figure4.12. The slope map gives a nice picture of how the waves shape the outermost part of the beach, indicating the change in the topography of the beach under seawater erosion by at least two years of images. In addition, the slope map clearly shows the boundary of buildings, trees, etc (purple). and the steeper section down to the sandy beach. Because buildings and trees are not in the study area, the study area can be better distinguished from irrelevant buildings based on the boundary line generated by the slope. The wave-like erosion caused by the erosion of seawater on coastal beaches is also clearly shown in the Slope map, as shown in Figure4.12. The slope maps of different years are also created, which can show the degree of seawater erosion of the beach according to the changes in slope.

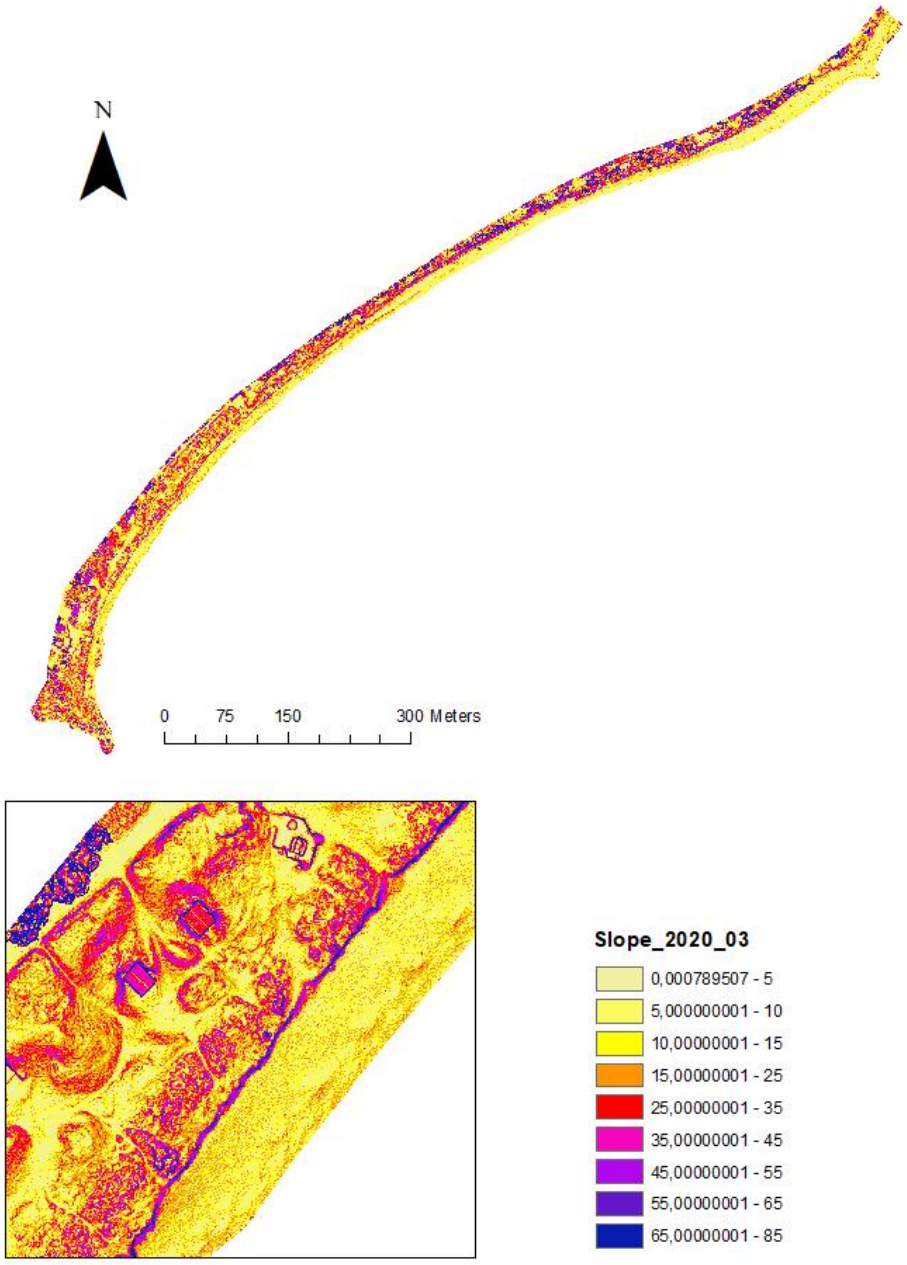

Figure.4.12 Slope Map (Data was taken on March 2020 by Kristianstad municipality)

5.Discussion

This study demonstrates that the DSM derived from UAV pictures allows for great planning flexibility and accuracy for coastal erosion monitoring and can be used for coastal erosion monitoring. This study processed and analysed UAV photos from five flights done in 2017, 2019, and 2020, resulting in a visual representation of the spatial distribution of coast elevation changes. This work's results can achieve an accuracy of 0.3 m for generating DSM on beaches in coastal locations, which is close to the

precision of 0.35 m achieved by earlier studies (Francisco, Fernando & Patricio, 2017). The precision of the DSMs achieved in this study is constrained by several issues, one of which is the quality of UAV picture alignment and DSM synthesis. Algorithm and software processing errors are unavoidable when aligning UAV pictures with SfM. However, this accuracy can be programmed into the software, and image processing accuracy can be enhanced by employing alternative accuracy criteria (the align standard used in this project is high). The precision of GCP is the second factor. Because all GCP is used to georeference DSM, the accuracy of GCP provided by the municipality of Kristianstad may also limit the accuracy of DSM. Furthermore, the precision of GCP markers during georeferencing will have an impact on the accuracy of the produced DSM. Because GCP markers are manually selected when placing all UAV photos, errors are unavoidable; however, errors can be minimised to the greatest extent feasible by selecting the middle area of each GCP.

Before assessing beach elevation variations, the study area must be established. The orthomosaic built by Agisoft Metashape from UAV photos is useful for determining the research region. Because the ground features can be identified visually and the study area can be chosen. Following the creation of the DSM, the value of each pixel represents the elevation of the place, resulting in a raster image that lacks the properties of surface items. Masking out the water body and other noises for such an image to determine the study region is quite tough in this endeavour. The orthomosaic using UAV data, on the other hand, can be used to visually choose the target research region, which has the advantage of being quick and accurate.

Differences in beach elevation can more intuitively show the severity of coastal erosion. The accuracy of elevation change is affected by uncertainty in the DSM, but elevation errors are divided into two categories, representing positive error and negative error. Then group the positive error and the negative error at a fixed interval, so that it is better to analyze the degree of influence of the uncertain value. The analysis of elevation changes should be divided into the following four-time gaps: 05/2020-03/2020, 03/2020-04/2019, 12/2019-04/2019 and 12/2019-10/2017. These time intervals can

display both the seasonal differences of elevation and the elevation differences of the same season in different years. For different time gaps, the value of the elevation change is also different. The error and the elevation difference map should be combined to get the elevation change in different time gaps.

In this project, only the error of the DSM position in the GCP can be obtained, because only the elevation value of the GCP position has reference data. When analyzing the elevation differences map, it should be combined with the accuracy map to quantify. It is to select two accuracy maps with the same time as in the elevation difference map calculation, and select the GCP error near the target area to calculate the absolute error of the area. The absolute error is to compare the errors in a vector manner. If the directions of the two errors are the same, the absolute error is equal to the subtraction of the absolute values of the two errors; if the directions of the two errors are opposite, the absolute error is equal to the sum of the absolute values of the two errors.

Analyzing the elevation difference maps of the four-time gaps respectively, it can be found that there are seasonal patterns and spatial patterns in actual coastal erosion. In the first-time interval (05/2020-03/2020), it can be seen from Figure4.3 that in the short time interval in spring, the beach elevation changes are mainly concentrated in two areas and are positive. This Represents that the beach obtains sediment from the ocean. According to the meteorological conditions, it can be known that the wind direction on 03/2020 is south and the wind direction on 05/2020 is north. The wind direction will affect the waves. The difference in the waves causes the imbalance of the sediments moved by whom, the input is greater than the output, and the beach at this time the elevation increases. But only the wind conditions on the day of the flight are known instead of the conditions between the flights. In the second time interval (03/2020-04/2019), it can be seen from Figure4.11 that the elevation of the beach has a zoning phenomenon, that is, the sediments in a small area in the south and north of the beach are lost and their upper beaches have gained sediment. This may be a phenomenon of Longshore current. When there is a certain angle between the direction of wave motion

and the coast, Longshore current is a phenomenon of the material moving along the coast (Niven & Bardsley, 2012). Therefore, in the same time interval, a part of the beach lost sediments while the nearby area grained sediments. In the third time interval (12/2019-04/2019), it can be seen from Figure4.6 that the elevation changes in the study area are mainly distributed in the central and northern parts, and there are also Longshore current phenomena. It can also be seen from the figure that the area closer to the seawater is more disturbed by the seawater, and the greater the elevation change. The fourth time interval (12/2019-10/2017) is relatively long and has similar climatic conditions. It is found from the map (Figure4.9) that the elevation of most areas is decreasing, except for the northernmost bay of the study area.

In addition to the elevation difference map, the DSM created from the UAV image can also be further processed and analyzed by ArcMap to obtain the slope map of the beach in the study area. An advantage of the slope map is that it can visually display the slope of the study area, thereby showing the topography of the study area. For example, Figure5.1 is the slope map of the same area in 2020 and 2017. Several obvious features of coastal erosion can be obtained from the figure. One is the “steep slope” on the beach, which is a steep slope formed by the continuous accumulation of sand due to the continuous erosion of seawater. You can see from the right picture that the "purple line" in this area is not obvious, while in the left picture there is a very obvious purple line between the building and the sandy beach. In Figure 5.2 and Figure 5.3, this is the profile of the blue line in the slop map. From these profiles, we can also see the emergence of steep slopes from 2017 to 2020. The other is the change in the slope of the beach. The width of the beach in these two pictures is different. This is due to the different time the UAV image was taken and the influence of the tide. However, the change of the slope can be seen from the change of seawater to the sandy beach. For example, compared with the right of the picture, a part of the area with a larger slope becomes flatter. This is because the seawater invades the land along the flat sandy beach. The washed sand is brought back to the ocean, leading to the expansion of the flat area

of the beach, and the erosion of the seawater will be further intensified.

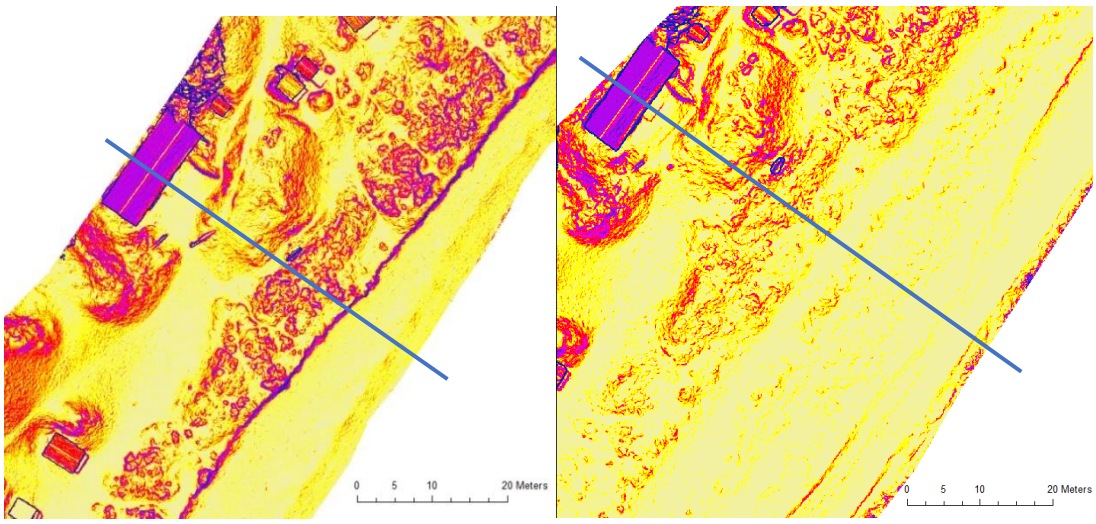

Figure5.1 Detail of Slope map of 03/2020(left) and 10/2017 (right)

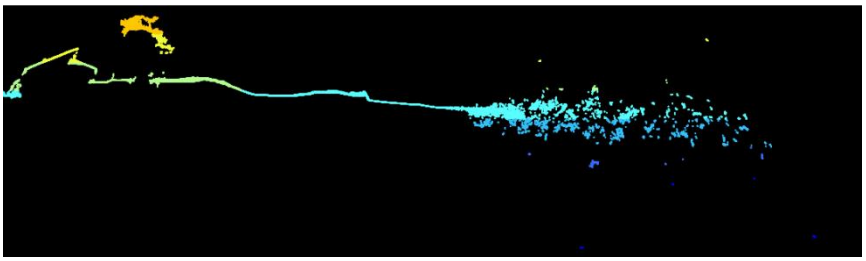

Figure5.2 Profile of March 2020 (blue line area)

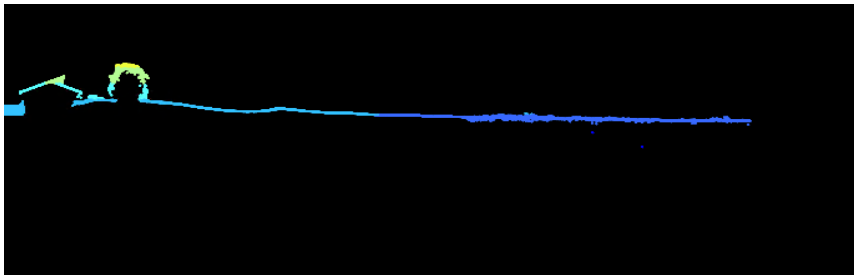

Figure5.2 Profile of October 2017 (blue line area)

This project uses UAV images to initially study the elevation differences of sandy beaches. Although there are still many errors and limitations, it also quantifies coastal erosion to a certain extent. It provides a good method for future coastal erosion monitoring. If algorithms can be used to reduce errors in data processing, UAV

measurement has a good application prospect.

In general, coastal erosion has been happening all the time. The lives and buildings of tens of millions of people are threatened by coastal erosion. Coastal erosion monitoring is very necessary. The application of UAV in coastal erosion monitoring not only reduces the cost of large-area coastal erosion monitoring but also produces DSM with higher temporal and spatial resolution and can further process DSM and conduct various studies on coastal erosion. Although UAV is still limited by battery power and weather conditions when performing large-area photogrammetry, UAV can still play an important role in monitoring coastal erosion and has great potential.

I have some suggestions for future work for Kristianstad municipality, the first is to plan a fixed measurement time. It is best to conduct two or four UAV flights within a year so that UAV data at fixed intervals can be obtained. A large amount of data can help to monitor coastal erosion and possibly predict the spatial distribution of coastal erosion based on time series. Then, when selecting the distribution of GCPs, it is best to be evenly distributed across the beach, so I think it can improve the accuracy of DSM.

6.Conclusion

The main focus of this project was to conduct research on elevation variations in the study area over different time intervals, seasonal patterns in changes, and spatial patterns in changes. The differences map is made for different time intervals (half a year, one year, and two years) and DSM while assessing elevation changes of the research area in different time gaps. The elevation variations in the results are aggregated and merged with DSM accuracy in different regions to assess elevation changes that occur over time. The data contain unclear numbers, but the shifting trend of elevation can still be noticed, which can help with coastal erosion monitoring.

It is discovered that there exist seasonal laws and spatial rules while examining numerous elevation difference maps. Waves, both constructive and destructive, have an impact on the seasonal rhythm. Sediments are primarily gathered in the spring and summer, and from spring to winter, distinct patterns will emerge in particular places based on the geography of the shore, but the seasonal variation is not particularly great. The longshore current can be seen to have an effect on the spatial pattern. The sand loss area is adjacent to the sand rise area and is affected by the direction of the waves, which is a general distribution feature.

Furthermore, by comparing the created slope map, the growth pattern of coastal erosion and topographical variations may be shown. Although coastal erosion cannot be quantified, the slop map provides a decent depiction of the phenomenon, and its occurrence may be observed intuitively.

After all, by comparing different UAV paths, the height change of the beach may be assessed, as can the degree of coastal erosion, as well as the seasonal and geographic patterns of height change. As a result, UAVs can provide significant benefits to coastal monitoring and forecasting.

Reference

A. Clark, (2017). Small unmanned aerial systems comparative analysis for the application to coastal erosion monitoring, GeoResJ, Volume 13, 175-185,ISSN 2214-2428. https://doi.org/10.1016/j.grj.2017.05.001

Adelaide's Coastal Erosion, (2015). Coastal Erosion Explained. Adelaide's Coastal Erosion. https://adelaidescoasterosion.wordpress.com/

Anthony E.J., (2019). Beach Erosion. In: Finkl C.W., Makowski C. (eds) Encyclopedia of Coastal Science. Encyclopedia of Earth Sciences Series. Springer, Cham. https://doi.org/10.1007/978-3-319-93806-6_33

BBC, 2015. Technical limitations of drones. BBC ACADEMY 4 Oct. 2015. https://www.bbc.co.uk/academy/en/articles/art20151214151812855

Burrough, P. A., and McDonell, R. A., (1998). Principles of Geographical Information Systems (Oxford University Press, New York), 190 pp. https://webapps.itc.utwente.nl/librarywww/papers_2009/general/principlesgis.pdf

C. Brouwer, 1985. Elements of Topographic Surveying, Irrigation Water Management: Training Manual, Measuring distances. http://www.fao.org/3/r7021e/r7021e04.htm

Casella, E., Rovere, A., Pedroncini, A. et al., (2016). Drones as tools for monitoring beach topography changes in the Ligurian Sea (NW Mediterranean), Geo-Mar Lett 36: 151. https://doi.org/10.1007/s00367-016-0435-9.

Central Intelligence Agency., (2021). Geography Sweden. The World Factbook. https://www.cia.gov/the-world-factbook/countries/sweden/

C. Flener, M. Vaaja, A. Jaakkola, A. Krooks, H. Kaartinen, A. Kukko, et al. (2013). Seamless mapping of river channels at high resolution using mobile liDAR and UAV-photography Remote Sensing, 5 (12), pp. 6382-6407. http://doi.org/10.3390/rs5126382

C.H. Hugenholtz, N. Levin, T.E. Barchyn, M.C. Baddock. (2012). Remote sensing and spatial analysis of aeolian sand dunes: A review and outlook. Earth-Science Reviews, 111 (3-4), pp. 319-334. http://doi.org/10.1016/j.earscirev.2011.11.006

Cooper, J.A.G. and Lemckert, C., (2012). Extreme sea-level rise and adaptation options for coastal resort cities: A qualitative assessment from the Gold Coast, Australia. Ocean & coastal management, 64, 1-14.

DHI., (2018). Erosionsutredning Kristianstad, Kristianstads kommun. https://www.kristianstad.se/contentassets/222f0391427c4cc2928d6e4b9266f924/Erosionsutredning_kust_havsplan.pdf , last accessed:18/05/2021.

F. Mancini, M. Dubbini, M. Gattelli, F. Stecchi, S. Fabbri, G. Gabbianelli, (2013). Using Unmanned Aerial Vehicles (UAV) for High-Resolution Reconstruction of Topography: The Structure from Motion Approach on Coastal Environments. Remote Sensing, 5 (12), pp. 6880-6898. http://doi.org/10.3390/rs5126880

Furukawa, Y., Curless, B., Seitz, S. M., and Szeliski, R., (2010) Towards internet-scale multi-view stereo, IEEE Comp. Soc. Conf. on Comp. Vis. and Patn. Recog, San Francisco, CA, 1434–1441, https://doi.org/10.1109/CVPR.2010.5539802

Francisco Agüera-Vega., Fernando Carvajal-Ramírez., and Patricio Martínez-Carricondo., (2017). Accuracy of Digital Surface Models and Orthophotos Derived from Unmanned Aerial Vehicle Photogrammetry. Journal of Surveying Engineering, Volume 143 Issue 2.

DOI:10.1061/(ASCE)SU.1943-5428.0000206

Goncalves, J.A., Henriques, R., (2015). UAV photogrammetry for topographic monitoring of coastal areas. ISPRS J. Photogrammetry Remote Sens. 104, 101–111.

RISC-KIT., (2021), KRISTIANSTAD AND ÅHUS, SWEDEN, RISC-KIT., https://coastal-management.eu/node/218

Haala, N. and Rothermel, M., (2012). Dense Multi-Stereo Matching for High Quality Digital Elevation Models. PFG Photogrammetrie, Fernerkundung, Geoinformation Jahrgang, Heft 4, 331-343, 2012.

INTERNATIONAL CIVIL AVIATION ORGANIZATION(ICAO), (2011). Unmanned Aircraft Systems (UAS). ISBN:978-92-9231-751-5.

J.A. Gonçalves, R. Henriques, (2015). UAV photogrammetry for topographic monitoring of coastal areas, ISPRS Journal of Photogrammetry and Remote Sensing, Volume 104, 101-111, ISSN 0924-2716, https://doi.org/10.1016/j.isprsjprs.2015.02.009.

L.C. van Rijn. (2011). Coastal erosion and control, Ocean & Coastal Management, Volume 54, Issue 12, 867-887, ISSN 0964-5691, https://doi.org/10.1016/j.ocecoaman.2011.05.004.

Lee, Y.K.; Eom, J.; Do, J.D.; Kim, B.J., and Ryu, J.H., (2019). Shoreline movement monitoring and geomorphologic changes of beaches using Lidar and UAVs images on the coast of the East Sea, Korea. Journal of Coastal Research, Special Issue, 90, 409-414.

Leo C Van Rijn, (1993). Principles of sediment transport in rivers, estuaries and coastal seas / Leo C. van Rijn - Amsterdam: Aqua Publications - I11. ISBN 90-800356-2-9 bound

Lowe, D. G. (2004). Distinctive image features from scale-invariant keypoints, Int. J. Comput. Vision, 60, 91–110, https://doi.org/10.1023/B:VISI.0000029664.99615.94.

Long, N., Millescamps, B., Pouget, F., Dumon, A., Lachaussée, N., and Bertin, X., (2016). ACCURACY ASSESSMENT OF COASTAL TOPOGRAPHY DERIVED FROM UAV IMAGES, Int. Arch. 45 Photogramm. Remote Sens. Spatial Inf. Sci., XLI-B1, 1127-1134, https://doi.org/10.5194/isprsarchives-XLI-B1-1127-2016.

M A Marfai, Sunarto. N Khakim , A Cahyadi , F S C Rosaji , H Fatchurohman, and Y A Wibowo,(2017). Topographic data acquisition in tsunami-prone coastal area using Unmanned Aerial Vehicle (UAV). *Earth and Environmental Science 148 (2018) 012004* doi :10.1088/1755-1315/148/1/012004

National Ocean Service., (2017). Longshore Currents. https://oceanservice.noaa.gov/education/tutorial_currents/03coastal2.html. Last accessed: 21/05/2021.

Niamh Danielle Cullen, Ankit Kumar Verma, and Mary Clare Bourke. (2018). A comparison of structure from motion photogrammetry and the traversing micro-erosion meter for measuring erosion on shore platforms. Earth Surf. Dynam., 6, 1023–1039, https://doi.org/10.5194/esurf-6-1023-2018.

Niven, RJ & Bardsley, DK. (2012). Planned retreat as a management response to coastal risk: a case study from the Fleurieu Peninsula, South Australia', Reg Environ Change, vol. 10, pp. 193-209.

Nissen, E., Arrowsmith, J. Ramon, Crosby, C., (2016). Introduction to Structure-from-Motion. http://kb.unavco.org/kb/file.php?id=810, Last accessed on 2018-11-07.

Neumann, Barbara & Vafeidis, Athanasios & Zimmermann, Juliane & Nicholls, Robert. (2015).

Future Coastal Population Growth and Exposure to Sea-Level Rise and Coastal Flooding - A Global Assessment. PLoS ONE. 10. 10.1371/journal.pone.0118571.

N.J. Rosser; D.N. Petley; M. Lim; S.A. Dunning; R.J. Allison, (2005). Quarterly Journal of Engineering Geology and Hydrogeology (2005) 38 (4): 363–375. https://doi.org/10.1144/1470-9236/05-008

Reid, C., & Mathews, E. (1906). Coast Erosion. The Geographical Journal, 28(5), 487-495. doi:10.2307/1776033. https://doi.org/10.2307/1776033

SA Gulyaev, J.S. Buckeridge, (2004). Terrestrial methods for monitoring cliff erosion in an urban environment. Coastal Res, 20 (3), pp. 871-878. https://doi.org/10.2112/1551-5036(2004)20[871:TMFMCE]2.0.CO;2

Stephen P. Leatherman, Bruce C. Douglas, John L. LaBrecque, (2011). Sea level and coastal erosion require large-scale monitoring. Eos, Transactions American Geophysical UnionVolume 84, Issue 2 p. 13-16. https://doi.org/10.1029/2003EO020001

Tak, W.J.; Jun, K.W., Kin, S.D., and Lee, H.J., (2020). Using drone and LiDAR to assess coastal erosion and shoreline change due to the construction of coastal structures. In: Malvárez, G. and Navas, F. (eds.), Global Coastal Issues of 2020. Journal of Coastal Research, Special Issue No. 95, pp. 674-678. Coconut Creek (Florida), ISSN 0749-0208.

Turner, I. L., Harley, M. D., Drummond, C. D., (2016). UAVs for coastal surveying. Coast Eng. 114, 19–24.

Tofiq Hemin., (2019). Investigating the accuracy of Digital Elevation Models from UAV images in areas with low contrast: A sandy beach as a case study. Lund University. https://lup.lub.lu.se/student-papers/search/publication/8974938

Webster, T. (2012). Atlantic Climate Adaptation Solutions Association Solutions d'adaptation aux changements climatiques pour l'Atlantique Coastline Change in Prince Edward, (February).

Yoo,C.I., Oh,T.S,(2016). BEACH VOLUME CHANGE USING UAV PHOTOGRAMMETRY SONGJUNG BEACH, KOREA, Int. Arch. Photogramm. Remote Sens. Spatial Inf. Sci., XLIB8, 1201-1205, https://doi.org/10.5194/isprs-archives-XLI-B8-1201-2016.

Zhang, K., Douglas, B.C. & Leatherman, S.P. (2004). Global Warming and Coastal Erosion. Climatic Change 64, 41. https://doi.org/10.1023/B:CLIM.0000024690.32682.48

Appendix

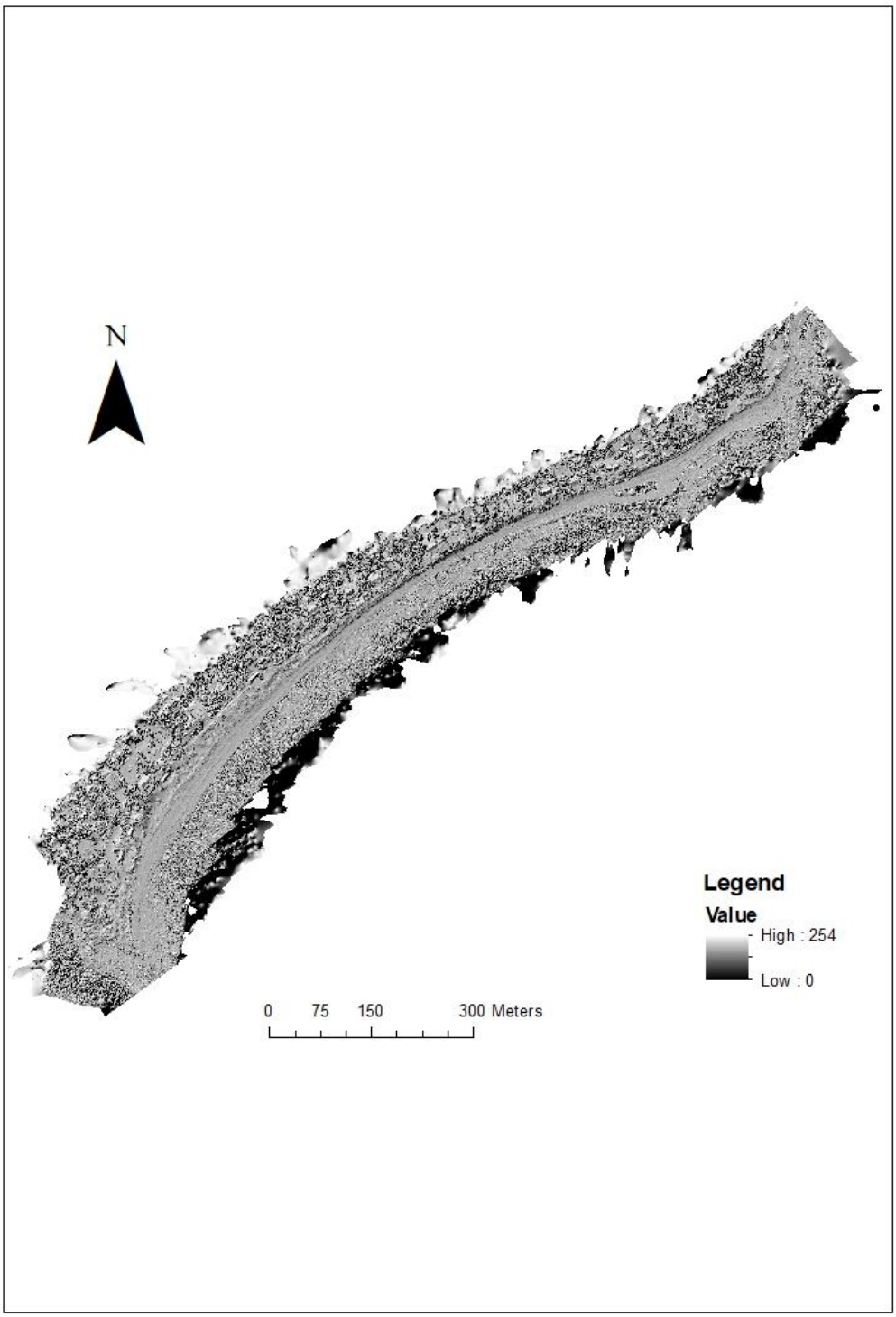

Figure.S1 Hillshaded DSM (Data was taken on October 2017 by Kristianstad municipality).

Approved for publication (spridningstillstånd), LM2021/020180.

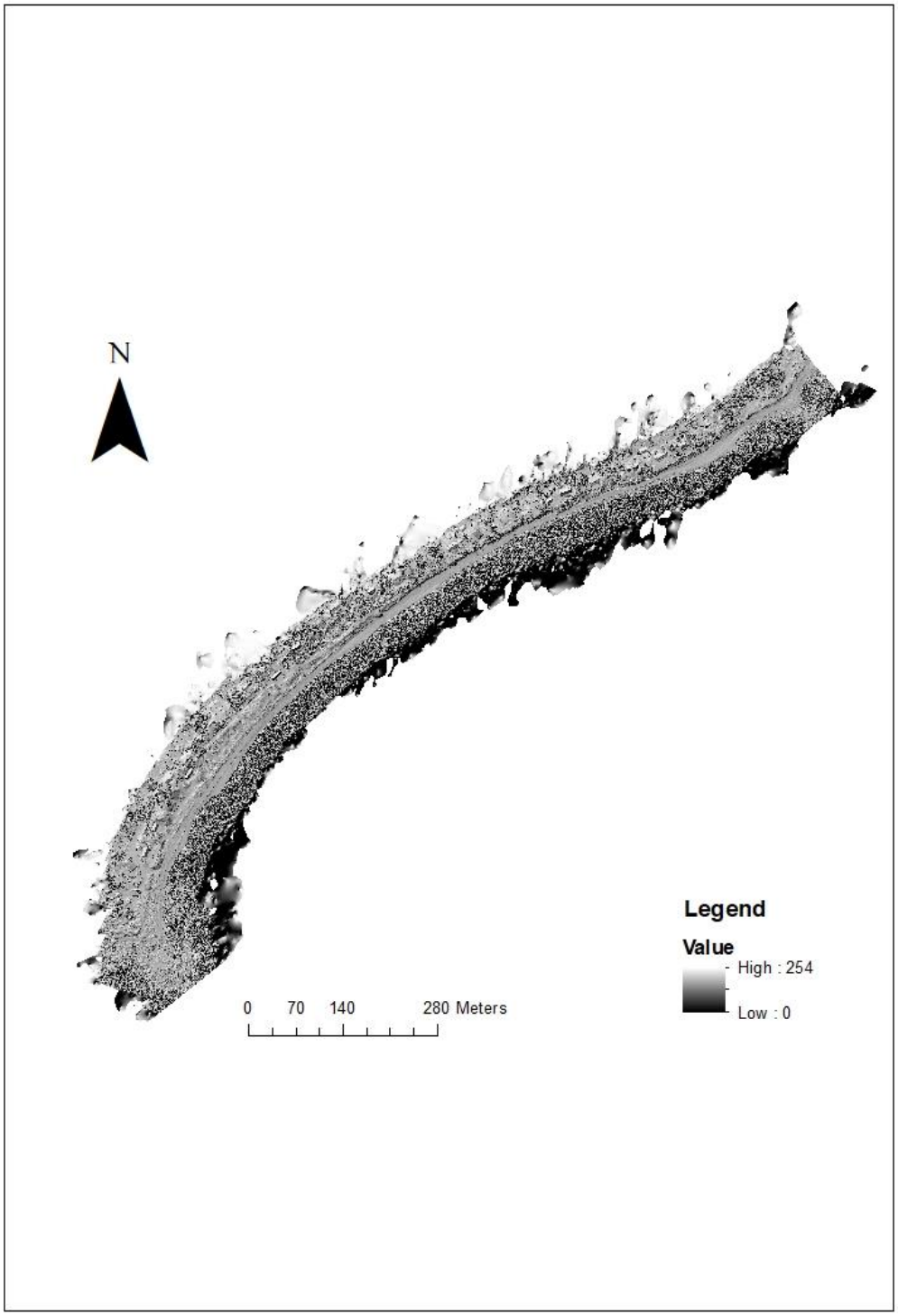

Figure.S2 Hillshaded DSM (Data was taken on April 2019 by Kristianstad municipality).

Approved for publication (spridningstillstånd), LM2021/020180.

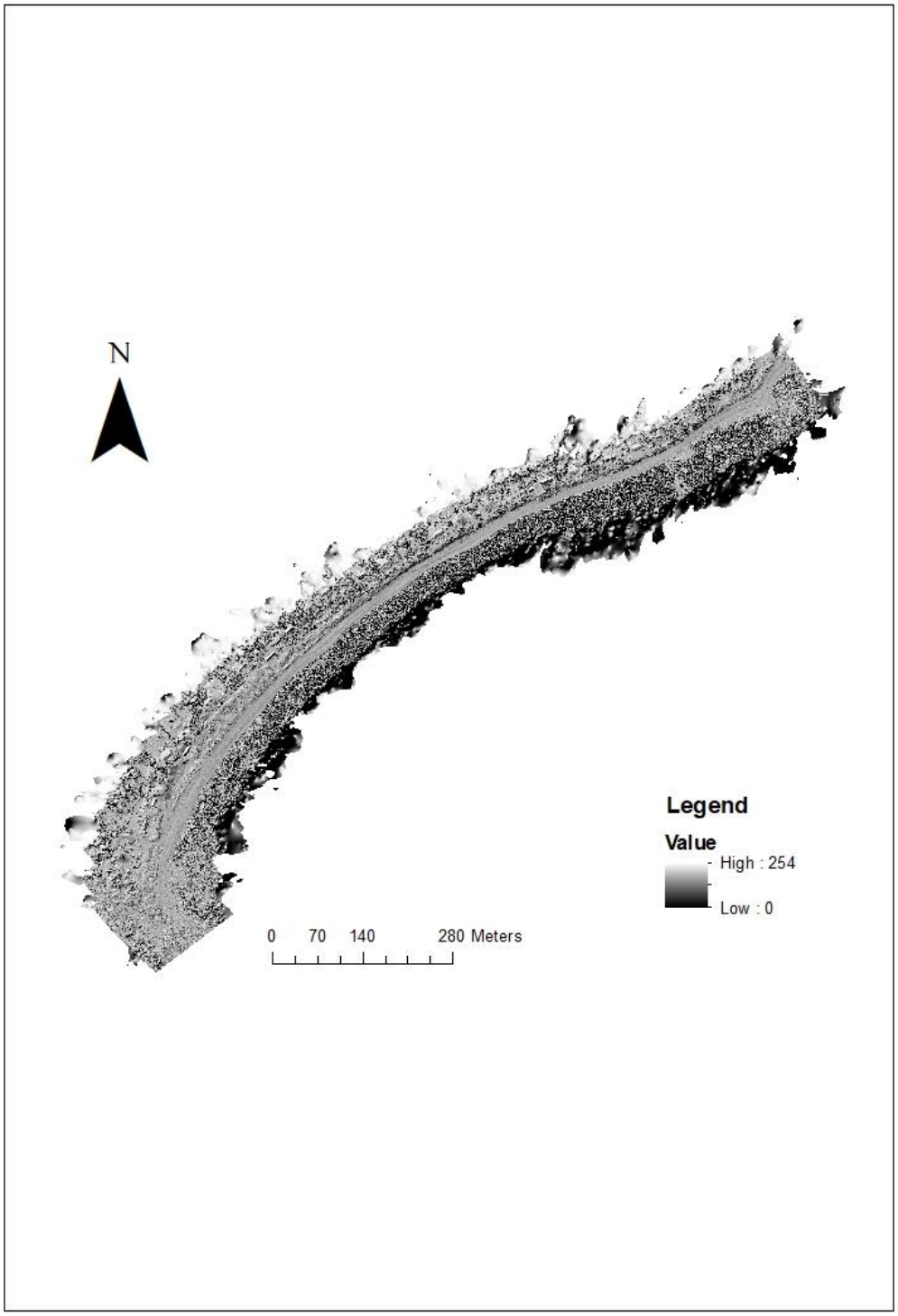

Figure.S3 Hillshaded DSM (Data was taken on December 2019 by Kristianstad municipality).

Approved for publication (spridningstillstånd), LM2021/020180.

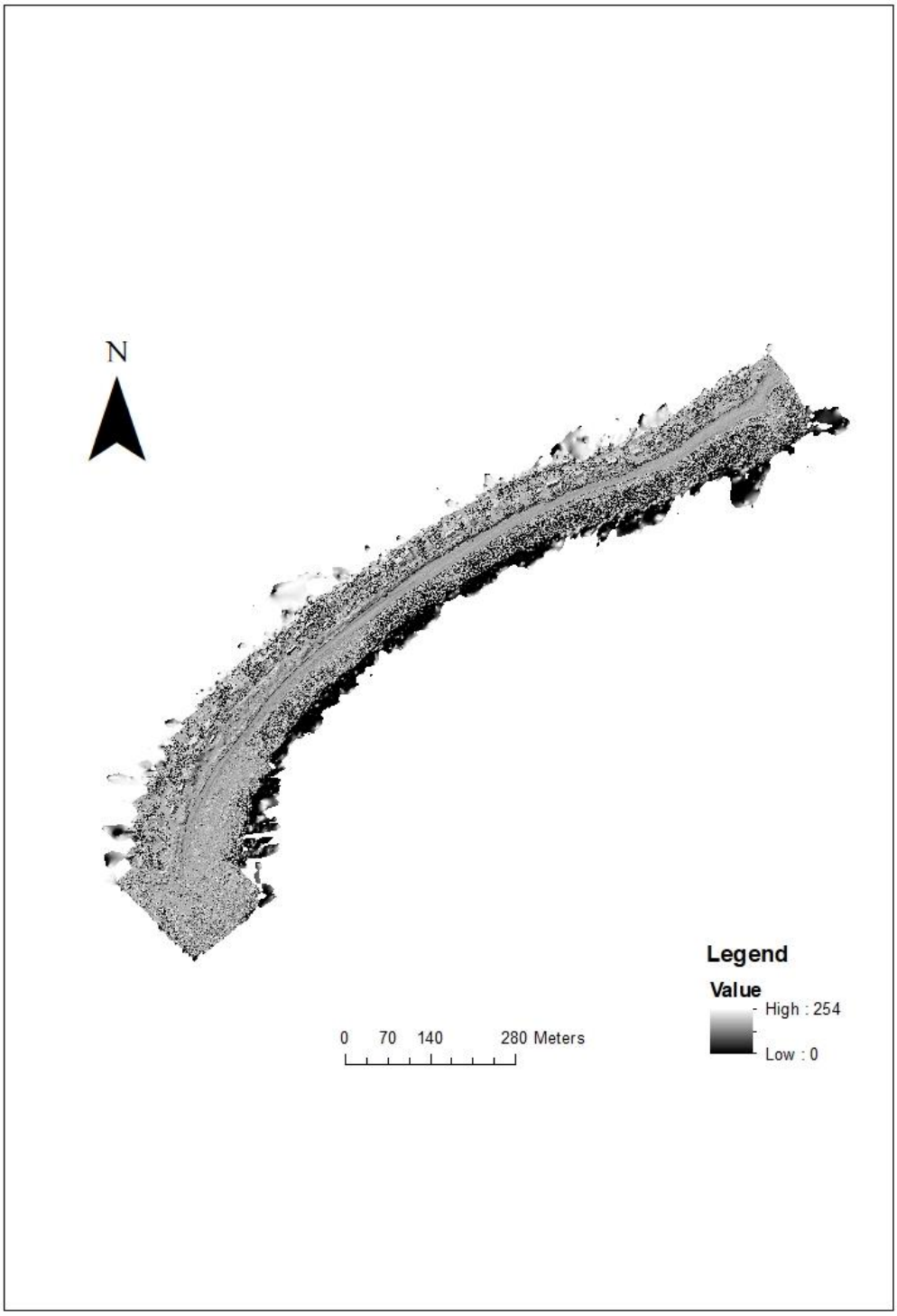

Figure.S4 Hillshaded DSM Hillshaded DSM (Data was taken on May 2020 by Kristianstad municipality). Approved for publication (spridningstillstånd), LM2021/020180.

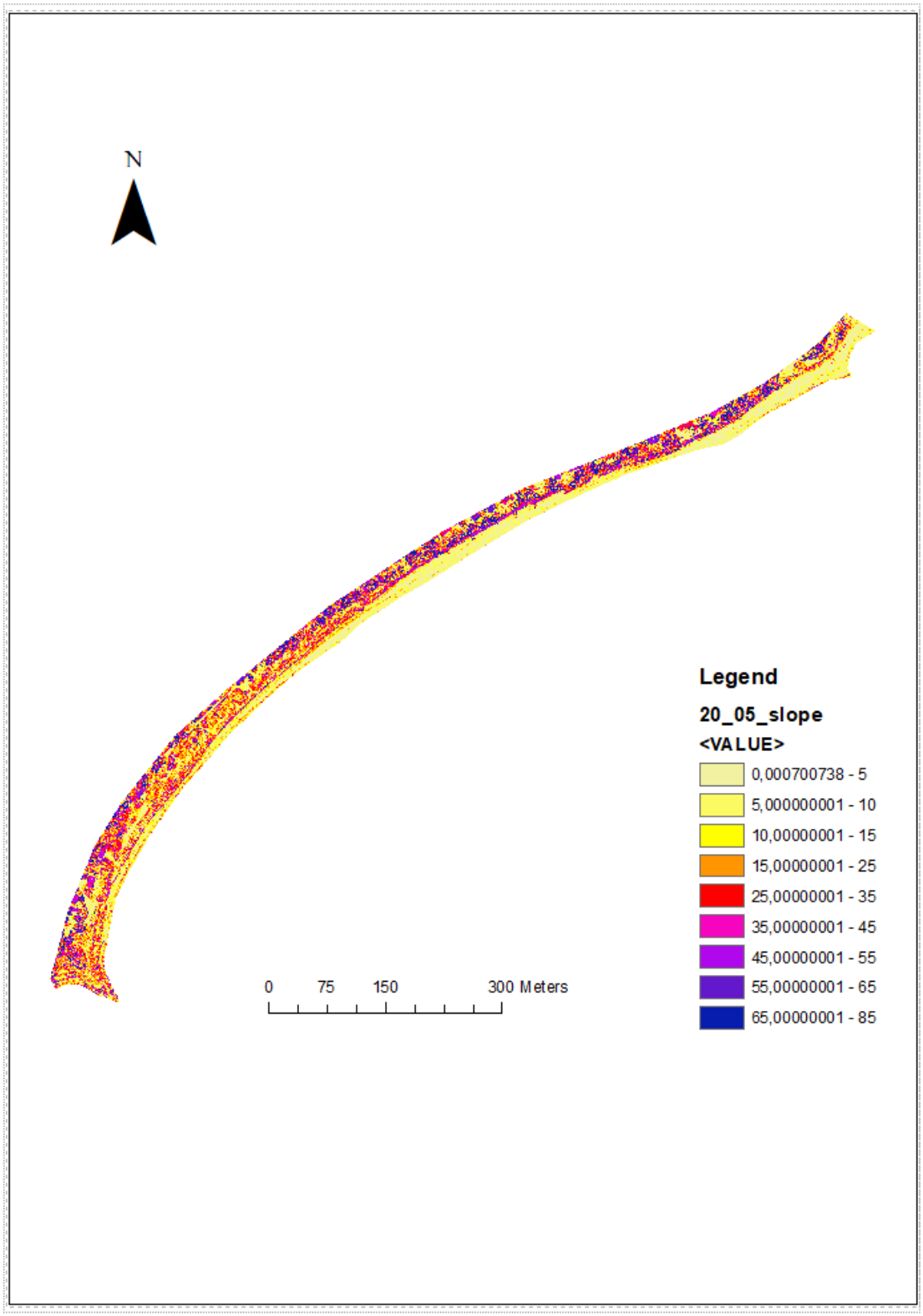

Figure.S5 Slope Map (Data was taken on May 2020 by Kristianstad municipality)

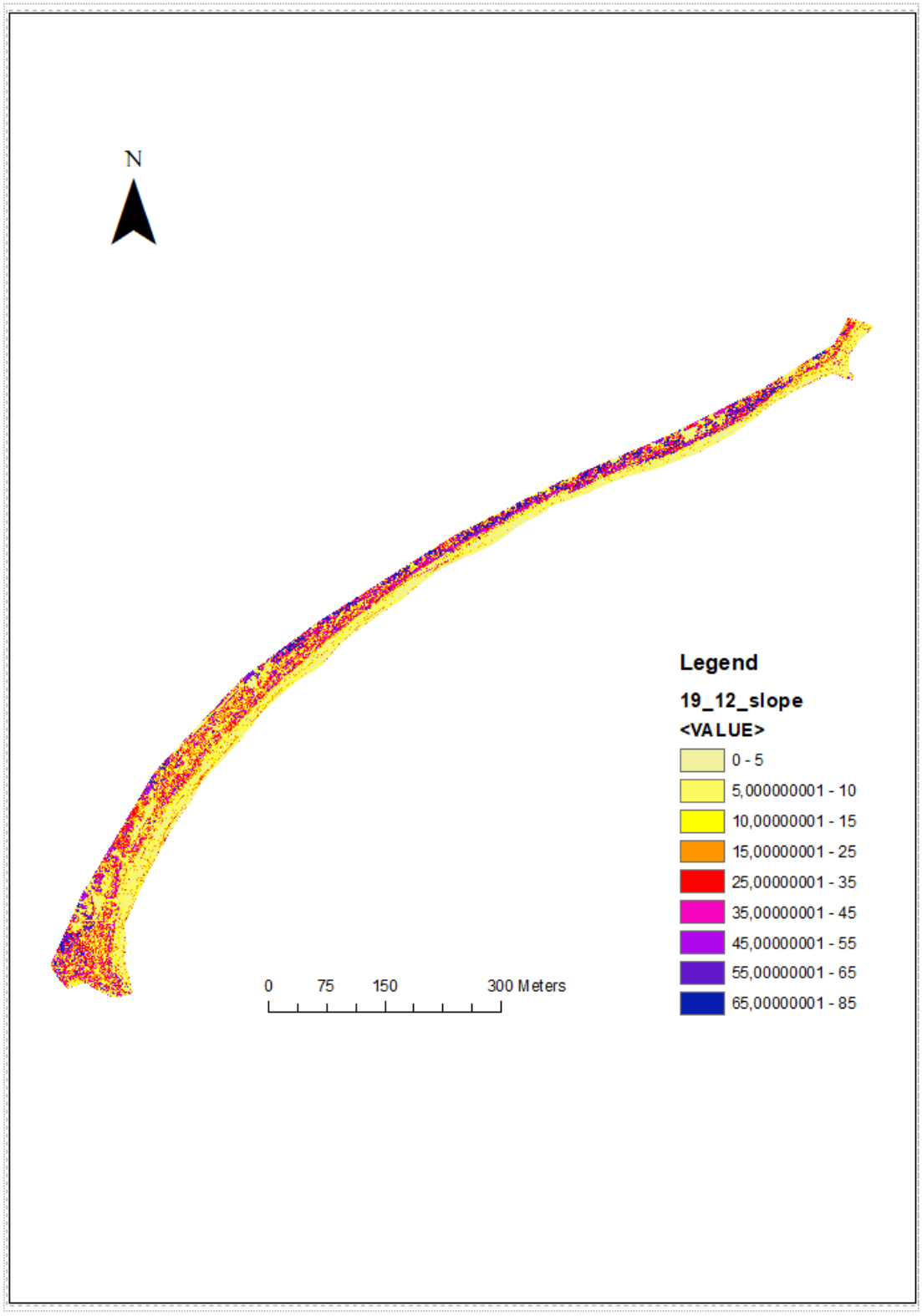

Figure.S6 Slope Map (Data was taken on December 2019 by Kristianstad municipality)

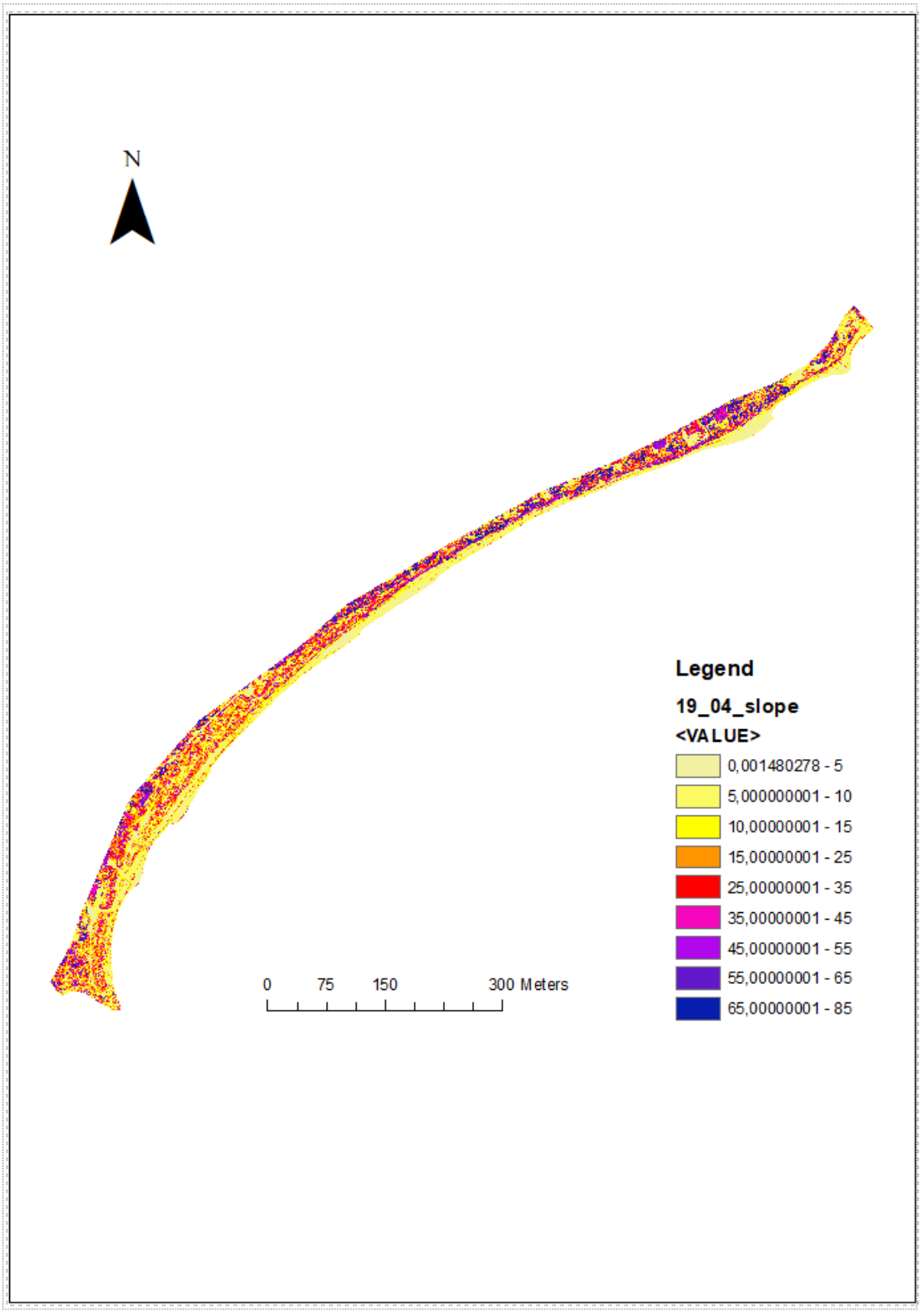

Figure.S7 Slope Map (Data was taken on April 2019 by Kristianstad municipality)

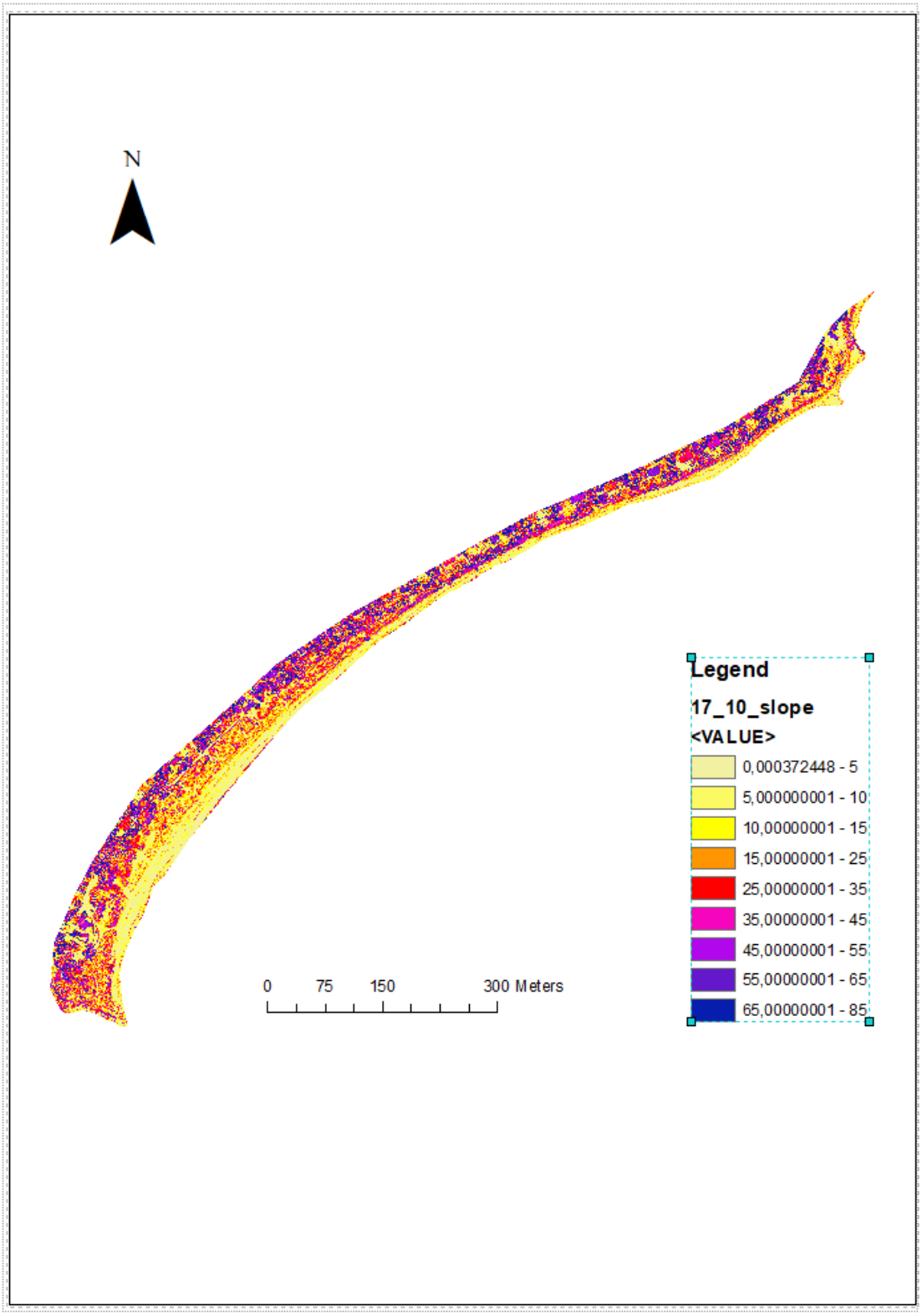

Figure.S8 Slope Map (Data was taken on October 2017 by Kristianstad municipality)